

Kinetic and Thermodynamic Studies on Adsorption of Sulphate from Aqueous Solution by Magnetite, Activated carbon and Magnetite-Activated Carbon Composites

Adegoke, H. I.^{1*}, Adekola, F. A.², Abdulraheem, M. N.¹

¹Department of Chemistry, University of Ilorin, P.M. B.1515, Ilorin, Nigeria

²Department of Industrial Chemistry, University of Ilorin, P.M.B.1515, Ilorin, Nigeria

e-mail: adegoke.hi@unilorin.edu.ng, tel: +234 7069365290

ABSTRACT

Magnetite nanoparticles, activated Carbon and their composites were synthesized in the laboratory. The adsorbents were characterized by bulk density, pH, pzc, surface area, iodine value, moisture contents, volatile components, Brunauer Emmett and Teller (BET) surface area, Scanning electron microscopy (SEM) coupled with Energy dispersive X-ray (EDX), X-ray Diffraction (XRD), Transmission Electron Microscopy (TEM) and Fourier transform infrared spectroscopy (FTIR). The adsorbents were employed for the batch adsorption of sulphate ion from aqueous solution. Some variable effects such as pH, initial concentration, contact time, adsorbent dosage and temperature on adsorption were also investigated. The data obtained were fitted into isotherms, kinetic model and thermodynamic process. The adsorption studies results revealed R^2 value ranging from 0.961 - 0.996 for Freundlich and Langmuir isotherm ranges from 0.954 - 0.979 for all types of adsorbents studied. Pseudo-first-order kinetic models correlation coefficient factor ranges between 0.818 - 0.947 while Pseudo-second-order kinetic models R^2 values ranges from 0.999 - 1. The equilibrium time for all adsorbent types range from 45-120 minutes and the maximum monolayer capacity (q_{max}) was observed to be between 83.0 - 142.86 mg/g for all the adsorbents at optimum pH 5. Thermodynamic studies revealed ΔH value to be in the range 1.484-4.573kJ/mol and ΔG value in the range -7.054- (-5.314) kJ/mol for all adsorbent types. Thermodynamic result revealed that the adsorption system was feasible, spontaneous and endothermic in nature

Keywords: Sulphate, Adsorption, Magnetite, Composites, Isotherm, Thermodynamic

INTRODUCTION

Drinking water is derived from a variety of sources depending on local availability; such as surface water (rivers, lakes, reservoirs and ponds), groundwater (aquifers) and rain water. These sources vary in terms of contaminants risk¹. The pollution of water resources due to the disposal of contaminants is an increasing worldwide concern for the last few decades. The most common water pollutants are inorganic and organic matters. They are discharged into the water by natural phenomenon or human activities ranging from discharge of effluents from municipal waste or industrial activities. Chemicals that are discharged into the surface and subsurface waters from these effluents are permeating environmental problem.

Sulphate is a naturally occurring substance that contains sulphur and oxygen. It is widely distributed in nature and may be present in natural water in concentration ranging from hundreds to several thousand mg/l. Sulphate is mostly found in soils and water and it has profound effect in environmental systems and technical applications, because it can alter the surface chemistry and crystal growth of iron oxides², poison catalysts, and affect the surface charge and reactivity of minerals such as sorption of anions and cations.

Sulphate is second to bicarbonate as the major anion in hard water reservoirs. It can be naturally occurring or the result of municipal or industrial discharges. When naturally occurring, they are often the result of the

breakdown of leaves that fall into a stream, or water passing through rock or soil containing barite (BaSO_4), epsomite ($\text{MgSO}_4 \cdot 7\text{H}_2\text{O}$) and gypsum ($\text{CaSO}_4 \cdot 2\text{H}_2\text{O}$)³. Municipal sources include sewage treatment plants and industrial discharges such as tanneries, pulp mills, and textile mills. Runoff from fertilized agricultural lands also contributes sulphates to water bodies.

Sulphates are of considerable concern because they are indirectly responsible for two serious problems often associated with the handling and treatments of waste water. They are odour and sewer corrosion problems which result from reduction of sulphates to hydrogen sulphide under anaerobic condition. The amount of sulphate in water is a factor of concern in determining the magnitude of the problems that can arise from reduction of sulphate to hydrogen sulphide.

The consumption of drinking water containing high amounts of magnesium or sodium sulphate may result in intestinal discomfort, diarrhoea and consequently dehydration. This laxative effect is often observed when someone drinks water that contains greater than 500 milligrams per litre (mg/L) of sulphate.

According to World Health Organisation (WHO) guidelines, sulphates in water to be used for certain industrial processes such as sugar production and concrete manufacturing must be reduced below 20 mg/l and recommended limits for water used as a domestic water supply are below 250 mg/L. Therefore, there is need to treat natural and industrial waste water that contains sulphate before discharge into the body of water.

Various technologies such as solvent extraction, ion exchange filtration and membrane separation, reverse osmosis, chemical precipitation and coagulation, have been proposed and evaluated for the removal of contaminant from aqueous solutions^{4,5}. These methods are known for one shortcoming or the other, ranging from

incomplete removal, high energy consumption, reagents cost, disposal of large volume of organic solvents and inefficiency when the metal concentrations are 10 mg/l⁶. Adsorption process is a promising alternative technique that is free from the shortcomings of the earlier techniques. Adsorbents from natural or modified materials and synthetic origin are subject of recent research efforts. These adsorbents include activated carbon from agricultural products^{7, 8} and oxides of iron⁹.

In recent time, nanotechnology has been used in many application including energy¹⁰, industries¹¹, sensor¹² and environmental application¹³. It provided fast and effective solution of many challenging problems that cannot be solved using conventional method due to generation of sludge into the environment¹⁴.

Magnetite -activated carbon nano-composite have been shown to be highly efficient materials for pollutants removal by adsorption¹⁵. To the best of our knowledge, there are limited reports found for the sulphate ion sorption onto Magnetite-activated carbon nano-composite which prompted us to investigate on it.

The aim of this research work is to synthesize and characterize magnetite nanoparticle, activated carbon and magnetite-activated carbon nano-composite for sorption of sulphate ion from aqueous solution.

MATERIALS AND METHODS

Sample Collection and Pretreatment

The coconut coir pith was collected from a coconut farm in Igbaye, Osun State, Nigeria. The collected coconut coir pith was properly washed with de-ionized water to remove any impurities deposited on the surface and sun dried prior to use.

Chemicals and Reagents

All reagents used in this research are of analytical grade and used without any further purification. These include de-ionized water (from SAM pharmaceutical Nigeria Ltd), NH₄OH, ferric chloride hexahydrate [FeCl₃·6H₂O] (97%), ferrous chloride tetrahydrate [FeCl₂·4H₂O] (99 %), sodium sulphate (Na₂SO₄) (Sigma Aldrich, Germany), isopropyl alcohol, glycerol, orthophosphoric acid (H₃PO₄), nitric acid (HNO₃), sodium Hydroxide (NaOH), barium chloride (BaCl₂), potassium nitrate (KNO₃), starch, iodine crystal (BDH) etc.

Synthesis of the Adsorbents

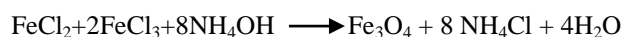
Synthesis of activated carbon

Activated carbon was synthesized by conventional heating method (carbonization), in which the heat is produced by electrical furnace. In this method, activated carbon was prepared through chemical activation of coconut coir pith precursor, using orthophosphoric acid as the chemical activating agent¹⁶. A 100 g of the coconut coir pith was ground using mortar and pestle to increase the surface area and carbonized at a temperature of 400 °C for 1 h in a stainless steel reactor placed in a furnace in the absence of air. The char produced was then activated with an aqueous solution of 1M concentrated phosphoric acid with an impregnation ratio of 1:5 (activating agent). The mixture was mixed in a mechanical mixer for 1 h to ensure the mixture was properly mixed. After that, the mixture was dehydrated in an oven at a temperature of about 105 °C for 24 hours, cooled to room temperature and washed with distilled water to remove any undiluted residue of ortho-phosphoric acid and then re-dried, ground and sieved in a glove box under nitrogen atmosphere to get the desired particle size and stored in plastic containers for further use. The product obtained was labeled ACT.

Synthesis of Magnetite (Fe₃O₄) nanoparticle

Magnetite nano-particle was synthesized by measuring 200 ml of deionized water into a round bottom flask deoxygenated by bubbling N₂ gas for 30 min. 50 ml of ammonium hydroxide (NH₄OH) (IM) was added and the mixture was stirred for 10 min at 1000 rpm using mechanical agitation. After which 10 ml of 0.1 M ferrous chloride (FeCl₂·4H₂O) and 20 ml of 0.1M ferric chloride (FeCl₃·6H₂O) was added in ratio 1:2 respectively; the reaction mixture generated a black precipitate immediately which was stirred and aged for 24 h before filtration¹⁷. The product obtained was washed severally with de-oxygenated- de-ionized water for it to be in pure form and then dried at 45°C for 4 hours. The product obtained was labeled MAG.

Chemical equation of reaction



Synthesis of Fe₃O₄-AC composites

The Fe₃O₄-activated carbon magnetic nanoparticles (AC-Fe₃O₄ MNPs) were synthesized in the ratio 1:3 and 1:5. 40 g of activated carbon was impregnated into nitric acid (63%) for 3 h at 80 °C in an ultrasonic bath. The sample was filtered, dried at room temperature and subsequently, 15 g and 25 g of obtained powder was weighed each into a 200 ml solution of Fe₃O₄ (this was obtained by in-situ method, the 200 ml of the suspension of prepared magnetite was measured without filtering) and placed in ultrasonic vibration for a 1 h at 80°C. The product formed was filtered, dehydrated in an oven at 105 °C for 1 h and then heated in a furnace at 750 °C for 3 h for the formation of AC-Fe₃O₄ magnetic nanoparticles. Finally, the synthesized adsorbent was washed with deionized water severally, then dried at 105 °C and kept in desiccators for use. The products obtained were labeled MAG-AC (1:3) and MAG-AC (1:5).

Characterization of the Adsorbents

The adsorbents were characterized by physico-chemical methods; bulk density, pH, point of zero charge (pzc) for the three adsorbents while iodine number, volatile, ash and fixed carbon contents was included for that of activated carbon. Spectroscopic analysis such as Scanning electron micrograph (SEM) was observed to know the morphology of the exterior surface of synthesized adsorbents, Energy dispersive X-ray to know the elemental composition present in the synthesized adsorbents, Transmission electron microscope (JEOL Model 1010 series), to confirm the morphology and the shape of the magnetite (Nanosizer to know sizes of the adsorbents, X-ray diffraction (GBC eMMA XRD model) was done using Cu-K α radiation, $\lambda = 1.54059 \text{ \AA}$ at 25°C to confirm the crystallinity nature of the magnetite and the composite. The specific surface area of the adsorbents was measured using BET surface area analyser (NOVA 4200) and the Fourier Transform Infrared (SHIMADZU) spectroscopy was used in order to determine the functional groups on the surface of the adsorbent over 500 – 4000 cm^{-1} .

Batch Adsorption Studies

Sorption experiments of sulphate ion were carried out by dissolving 1.479 g of Na₂SO₄ (Sigma-Aldrich) in 1000ml standards flask. Standard solutions of (0-800) mg/L were prepared serially from the stock solution prepared for the adsorption study. The determinations of the various standard concentrations were determined on a UV-visible spectrophotometer (SHIMADZU model) at a wavelength of 362 nm.

Adsorption of sulphate ion

0.1, 0.5 and 0.2 g of the magnetite, activated carbon and composite were made in contact each with 25 ml of sulphate standard solution prepared (0-800) ppm initial concentration and agitated on mechanical shaker for 240 minutes

after which they were filtered. All filtrates were prepared using conditioning reagent^{19, 20} to become turbid depending on the concentration of sulphate in the solution in order to measure sulphate concentration left after sorption. The final concentration of sulphate in solution was determined by measuring the absorbance at 362 nm by UV-VIS spectrophotometer (SHIMADZU model). Optimization of pH and contact time was performed within the range of 2.0 – 9.0 and 5 – 240 min, respectively. Then, the adsorption of sulphate under different amounts of adsorbent (0.02–1 g/L) and temperature (303 – 334 K) were studied, respectively.

The amount of adsorbed sulphate by the adsorbents were determined by equation

$$Q_e = \frac{v(C_i - C_f)}{m} \quad (1)$$

Where q_e is the adsorption capacity of adsorbent at a given time t (mg/g), V is the volume of solution (L), m is the mass of adsorbent (g) and C_i and C_f (ppm) are the initial and equilibrium concentration of sulphate, respectively.

Estimation of the adsorption isotherm and kinetics

In adsorption process, the study of equilibrium adsorption isotherm is the basis for the modeling of an adsorption system²¹. The Adsorption capacities of the adsorbents were determined by fitting the experimental results into Langmuir, Freundlich and Temkin isotherm represented by the following equations, respectively:

Fundamental thermodynamic parameters including standard enthalpy (ΔH°), standard free energy (ΔG°), and standard entropy (ΔS°) were all measured for thermodynamic studies. Van't Hoff plots were employed for the calculation of ΔH° and ΔS° based on the following equations:

$$K_c = \frac{q_e}{C_e} \quad (2)$$

$$\Delta G^{\circ} = -RT \ln K_c \quad (3)$$

$$\ln K_c = -\frac{\Delta H^{\circ}}{RT} + \frac{\Delta S^{\circ}}{R} \quad (4)$$

RESULTS AND DISCUSSION

Physico-chemical Characteristics

The percentage yield for the MAG, ACT MAG-AC (1:3) and

MAG-AC (1:5) ranged from 36.5 to 98.5 % with the MAG-AC (1:5) having the highest yield percent and MAG having the lowest yield percent as it can be seen in Table 1. The coconut coir pith could serve as a very good precursor for the production of activated carbon due to its very low value in ash content and moderate value of fixed carbon constituents. Moisture content, according to Azizian, 2004²² has a relationship with porosity (α) and yield according to Lori et al, 2007²³ of a given carbon. Adsorbent with high moisture content is expected to swell less, thus retarding pore size expansion for adsorbate uptake.

The moisture content of ACT was found to be 2.9 % while the volatile content was found to be of 38.5 %. This is responsible for the decomposition of the organic materials to release volatiles and development of microporous structures²⁴. Report has shown that low volatile matter content implies the high porosity of the adsorbent since volatile matter remains clogged in the carbon pores²⁵. Ash is a measure of inorganic impurities in the carbons²⁶. The ash content of activated carbon was found to be 3.8 % which is in the range of most ash content of agricultural waste reported²⁷.

Fixed Carbon content is the residual amount of carbon present in the sample. The result obtained shows that carbon content is 54.8 %. This is in concordance with the findings of Malik et al. 2006²⁴ in which most of the carbon composition of AC falls within 50-90 %.

The test of bulk density represents the flow consistency and packaging quantity of solid sample. The bulk density of any sample plays a great role on adsorbate uptake. Generally, higher density carbons hold more adsorbate per unit volume²⁸. From Table 3, the bulk density of the MAG is the highest (4.29 g/ml) and that of activated carbon is the lowest (1.07 g/ml). The higher bulk density of the MAG can be due to its compactness in nature because of its crystal form especially when in nano sizes are prone to agglomeration which makes the particle to tightly fuse together and occupy every available space.

The iodine number is the most fundamental parameter used to characterize activated carbon performance²⁹. It is a measure of activity level, the higher the number, the higher the degree of activation and the development of the microporous structure. It is often reported in mg/g. Iodine number may also be used as an approximation of surface area. Some types of carbons have been reported to be between 600 mg/g and 1100 mg/g^{30,31}. The iodine number of AC adsorbent was found to be 812.16 mg/g, this is in agreement with the report in the literature²⁹ where all the adsorbents have higher iodine number and higher degree of micropore, as an indication of better performance as adsorbents.

Surface area and micropore volume are the key factors in determining whether the material is suitable for the removal of pollutants from aqueous solutions. In addition, the nature of the adsorbent-adsorbate interaction must also be considered. It is understood that the pore volume contributed to the accommodation of metal ion on the adsorbent³².

Specific surface areas of the adsorbents were determined by the Brunauer–Emmett–Teller (BET) method. The BET isotherm is the basis for determining the extent of nitrogen adsorption on a given surface. The surface areas of MAG, ACT, MAG-AC (1:3) and

MAG-AC (1:5) composites were found to be 276.956, 833.641, 444.095 and 454.569 m²/g, respectively which falls within the range of their specific surface area with the pore volume and pore sizes of (10.97, 32.86, 17.27 and 15.73 cc/g) and 3.015, 3.148, 3.091 and 3.335 nm respectively. The surface area of the MAG, MAG-AC (1:3) and MAG-AC (1:5) are lesser than that of ACT. This decrease could be attributed to the occupation of almost the entire pores of AC with Magnetite nanoparticle resulting in less accessible pores²¹. The variation in surface area could also be as a result of chemical used. The surface areas of the samples are comparable with some of the commercial, synthetic and natural iron oxides reported in literature³³. The pH of adsorbents determined the kind of adsorbate its likely to remove in an adsorption system, whether there will be adsorption of H⁺ ions from the solution or desorption of OH⁻ ions from the sorbent surface when the adsorbent is basic or acidic³⁴. The pH of the synthesized ACT, MAG, MAG-AC (1:3) and MAG-AC (1:5) in

de-ionized water ranges from 6.3 to 8.0. ACT and the composites had their pH tend a bit towards acidic range; this could be attributed to the method of synthesis. The pH of the produced ACT was found to be 6.8, which falls within the range of pH of most agricultural by-products. This is also in agreement with the report of Mohammed et al, 2015²⁶. Generally, adsorbents with pH of 6-8 are acceptable in most applications³⁵. The pH of composites are lower (6.5 and 6.3) than that of ACT and MAG

The point of zero charge of a material facilitates the choice of an adsorbent for removal of certain solutes from waste water; it also makes it possible to predict the pH effect on the phenomena and processes involving adsorption³⁶.

The point of zero charge was located at point of interception of the curve. However, the points of interception for various ionic strengths (0.1, 0.01 and 0.001 M KNO₃) were in the range of 6.2 and 7.8 with MAG having the highest and activated charcoal been the least

Table 1: PHYSICO-CHEMICAL PROPERTIES OF MAG, ACT, MAG-AC (1:3) AND MAG-AC (1:5) ADSORBENTS

Physicochemical Parameters	Magnetite (MAG)	Activated carbon (AC)	MAG-AC composite (1:3)	MAG-AC composite (1:5)
Appearance	Black	Black	Black	Black
% Yield	36.65	60	96.5	98.5
Bulk Density (g/cm ³)	4.89	0.298	2.35	1.07
pH	8	6.8	6.5	6.3
PZC	7.8	6.2	ND	ND
Fixed carbon (%)	ND	54.8	ND	ND
Volatile component (%)	ND	38.5	ND	ND
Moisture content	ND	2.9	ND	ND
Ash content (%)	ND	3.8	ND	ND
Iodine Value	ND	812.16mg/g	ND	ND
BET Surface area (m ² /g)	278.956	833.641	444.	454.569
Micro-pore volume (cc/g)	1.097 × 10 ¹	3.286 × 10 ¹	1.727 × 10 ¹	1.573 × 10 ¹
Pore size (nm)	3.015	3.148	3.091	3.335

Spectroscopic characteristics of the adsorbents

XRD analysis was performed to examine the crystal structure of the synthesized MAG and MAG-AC (1:3). The typical XRD pattern of the adsorbents is shown in Fig. 1a and b.

From the spectra shown below for magnetite, peaks are found at positions of 6.07° , 19.04° , 35.85° , 40.70° , 54.13° and 63.49° which are in good agreement with values found in literatures [37, 38]. The appearance of a broad peak at $2\theta = 35.85^\circ$ [15, 27, 39] and 15.65 and 26.70 could be

interpreted as the evidence for the presence of Fe_3O_4 crystalline phase. The composite shows some distinct spectral which are found at peaks 15.65° , 22.66° , 26.70° and 39.87° because of the slight shift in the peaks due to activated carbon. The main peak at $2\theta = 15.65$ and 26.70° corresponds to carbon [40]. It can also be seen from the diffractograms obtained for MAG that it has a higher degree of crystallinity than that of the composite.

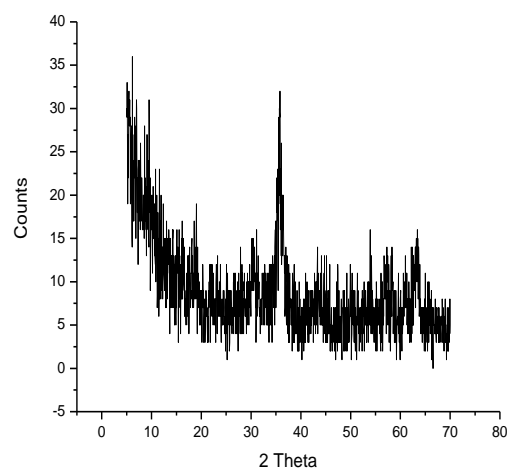


Figure 1a: X-ray Diffractogram of MAG

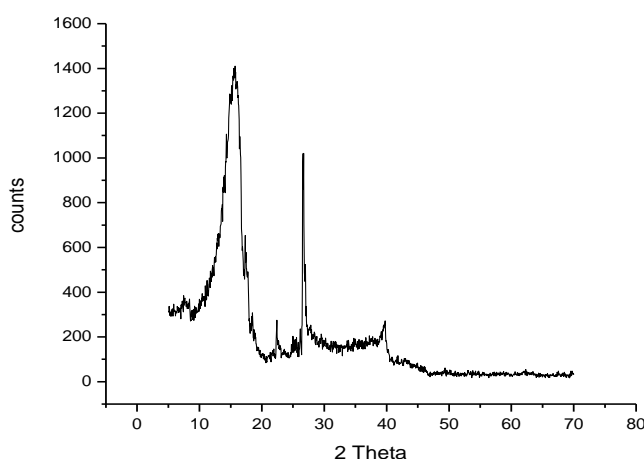


Figure 1b: X-ray Diffractogram of MAG-AC

Fourier Transform Infrared Spectroscopy (FTIR)

Fourier Transform Infrared Spectroscopy (FTIR) analysis was carried out in order to identify the functional groups present in the sample. Functional groups of adsorbents not only affect the adsorption behaviour, but also dominate the adsorption mechanism⁴¹.

The surface functional groups were characterized by Fourier transforms infrared (FT-IR) spectroscopy. Table 2 shows the FTIR spectra between $4,000$ to 500 cm^{-1} .

The FTIR spectra obtained for magnetite (MAG) is shown in Figure 2a and the detailed summary shown in Table 2. A broad absorption band at 3423.76 and 3223.16 cm^{-1} are due to the O-H stretching frequency. The

H_2O intra-molecular bending frequency gives the absorption band at 1647.21 cm^{-1} . The stretching frequency of Fe – OH is found at the 869.92 cm^{-1} and the peak at 628.81 cm^{-1} is due to the presence of O – H deformation bands found in magnetite. The absorption band at 449.43 and 567.09 cm^{-1} indicates the stretching frequency of Fe – O due to H_2O ⁴². All these characteristic peaks can be attributed to magnetite particle. The spectral obtained for the activated carbon (ACT) adsorbent is shown in Figure 2b and the detail are summarized in the Table 2. A broad absorption band at 3421.83 cm^{-1} is due to the surface O-H stretching frequency, while the C-H stretching

vibration at 2962.76cm^{-1} indicates the presence of alkane (sp^3) stretching vibration functional group. The peak found at 2362.88 cm^{-1} corresponds to the $\text{C}\equiv\text{C}$ stretching vibration of the alkyne functional group. The $\text{C}=\text{C}$ stretching vibrations at 1602.90 cm^{-1} is assigned to alkenes and aromatic stretching vibration functional groups. The peak at 1269.20 and 1217.12 cm^{-1} in the adsorbent corresponds to the C-H rock and C-H bend of the aliphatic functional group or C-O-H. The FTIR spectra obtained were in agreement with the results reported in the study carried out on commercial granular activated carbons by Jung et al;⁴³. This is also in agreement with the work of Tan et al. 2008⁴⁴

In the spectral of the composites shown in Figure 2c and d, the bands found in magnetite and the activated carbon are also present with just slight shifts due to the formation of new product from the primary reactants. The additional peaks found in composites apart from magnetite are shifted peaks due to presence of the activated carbon. The slight shifts in peaks are shown in Table 2, similar slight shift were observed for $\text{C}\equiv\text{C}$ stretching from 2362.88 to 2351.30 and 2360.95cm^{-1} for MAG-AC (1:3) and MAG-AC (1:5) respectively, C – H rock at 1269.30 to 1298 cm^{-1} for MAG-AC (1:3)

Table 2; Some fundamental bands observed in MAG, AC, MAG-AC (1:3) and MAG-AC (1:5)

Absorption Bands	Peaks found in MAG(cm^{-1})	Peaks found in AC (cm^{-1})	Peaks found in MAG-AC (1:3) (cm^{-1})	Peaks found in MAG-AC (1:5) (cm^{-1})
O-H stretching frequency	3423.76 and 3223.16	3421.83 and 3064.99	3479.70	3454.62
C - H (sp^3) stretching	-	2962		
Intramolecular H-OH frequency	2881.75	-	2831.60	2831
$\text{C}\equiv\text{C}$	-	2362.88	2351.30	2360.95
O-H bending mode	1624	-	1633.76	1627.97
$\text{C}=\text{C}$ stretching		1602.90	-	-
H_2O intramolecular bending frequency	1406.15	-	-	1398.44
C –H rocking	-	1269.20	1298	-
C – H bending	-	1217.12	-	1217.12
Fe-OH stretching frequency	869.92	-	875.71	875.71
O-H deformation	628.81 and 582.52	-	644.25	648.10
Fe-O stretching frequency of H_2O	449.43 and 567.09	-	569.02	574.81

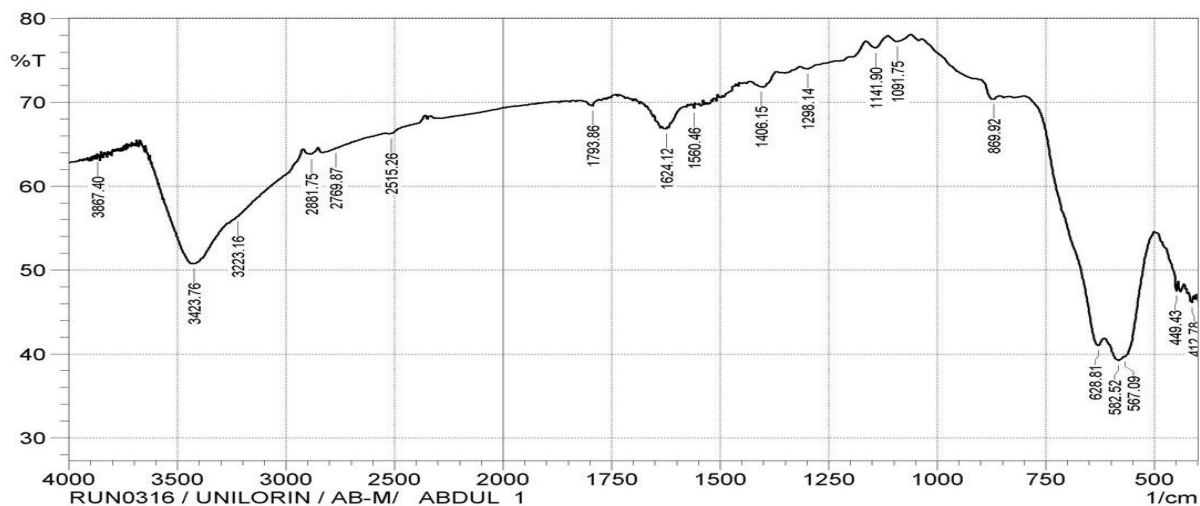


Figure 2a: FTIR spectrum of Magnetite

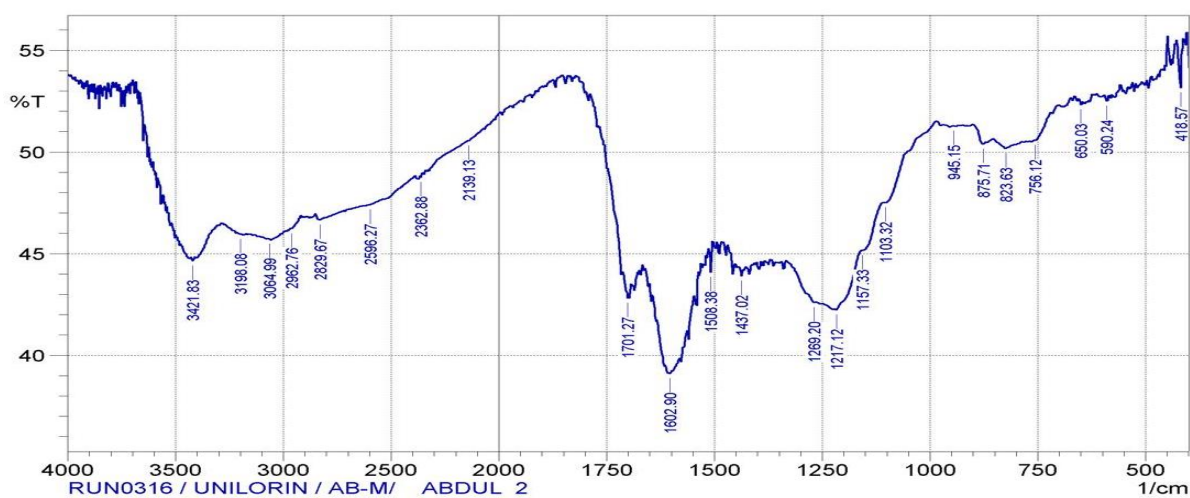


Figure 2b: FTIR spectrum of Activated carbon

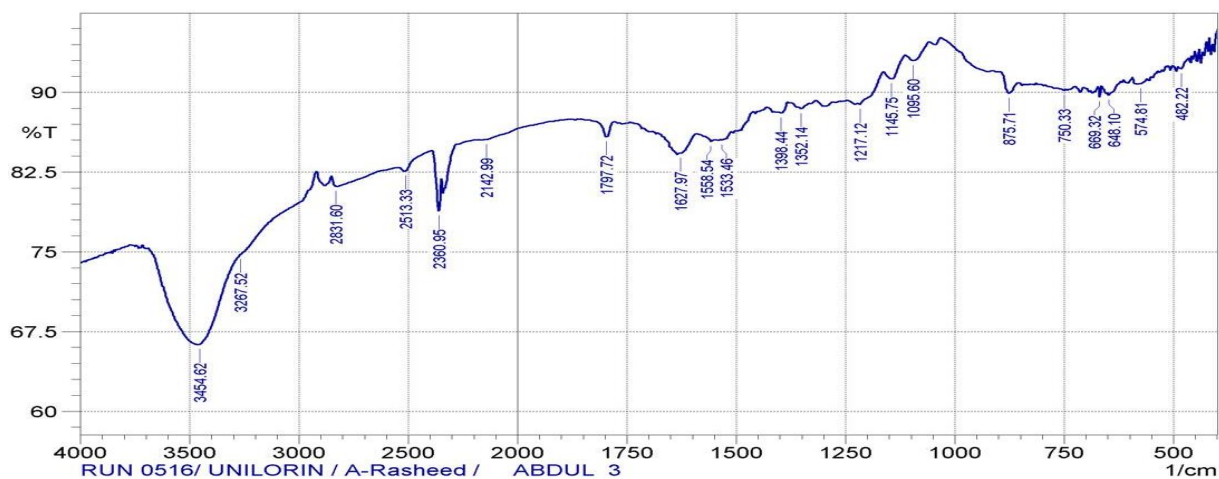


Figure 2c: FTIR spectrum of MAG-AC (1:5)

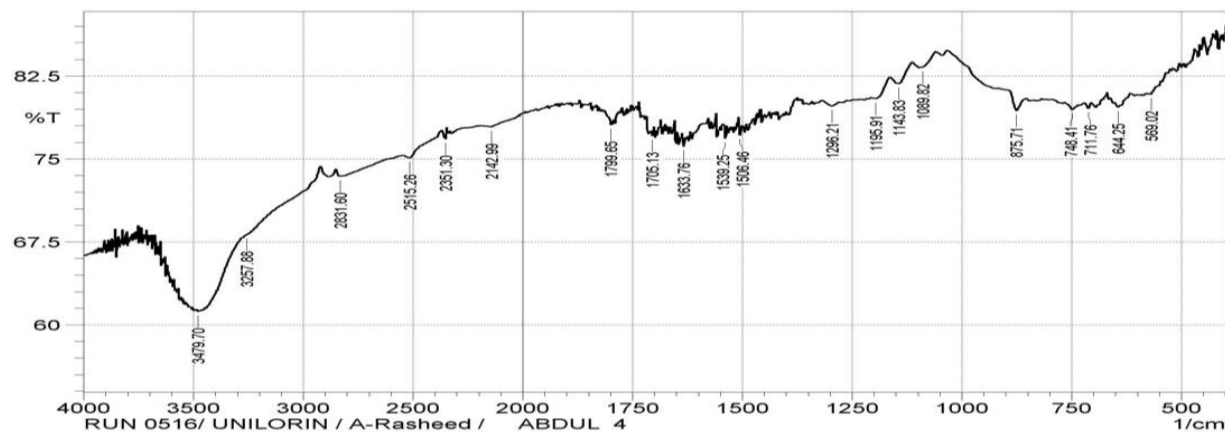


Figure 2d: FTIR spectrum of MAG-AC (1:3)

Scanning Electron Microscopy

The SEM micrograph of AC, MAG, MAG-AC (1:3) and MAG-AC (1:5) representing the surface morphology of the synthesized adsorbent is illustrated in Figure 3a. Large and well-developed pores which looks like honey comb were clearly found on the surface of the activated carbon. This might be due to the activation process used, which involved chemical activating agents of H_3PO_4 . Pore development in the char during carbonization was also important as this would enhance the surface area and pore volume of the activated carbon by promoting the diffusion of H_3PO_4 molecules into the pores and thereby increasing the H_3PO_4 carbon reactions, which would then create more pores in the activated carbon. This result is in agreement with some researcher's report^{27, 44}. MAG micrograph is shown in Figure 3b with the following features; particles are aggregates of small particles, non-

porous, with irregular shape (like triangle, plate-like), relatively smooth surface, and without cavities. These characteristic could be as a result of method of synthesis while the composites are porous in nature. The porous nature of the synthesized composites from activated carbon and magnetite is an implication of large surface area and high adsorption capacity. Formation of the magnetic-AC was confirmed by the presence of several mono-disperse magnetite nanoparticles embedded in activated carbon pores with needle-like shapes, large number of agglomeration, large pore sizes but not as large as activated carbon as a result of magnetite which was dispersed over the surface. This could be due to the fact that there were no pores on the surface of the magnetite which was expected to increase the surface area of the activated because of its nanoparticle nature. This result is in concordance with literature values²¹.

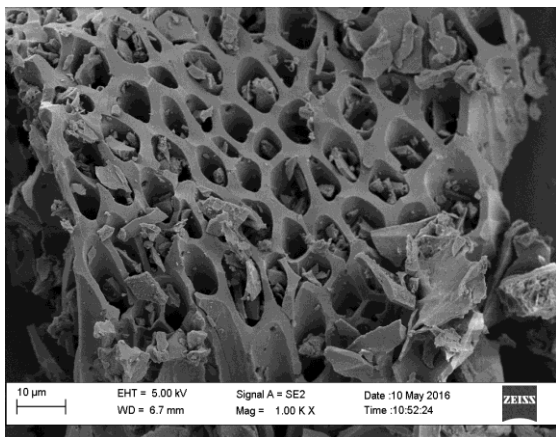


Figure 3a: SEM micrograph of (ACT)

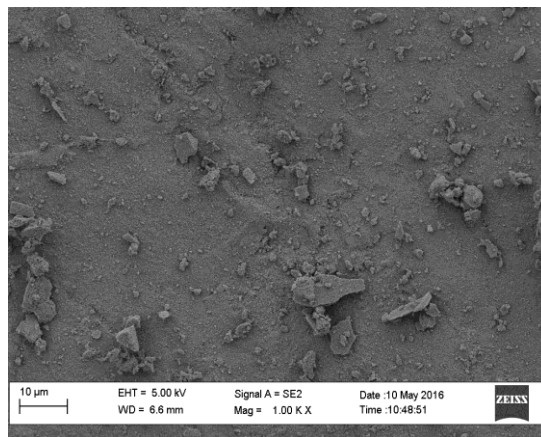


Figure 3b: SEM micrograph of (MAG)

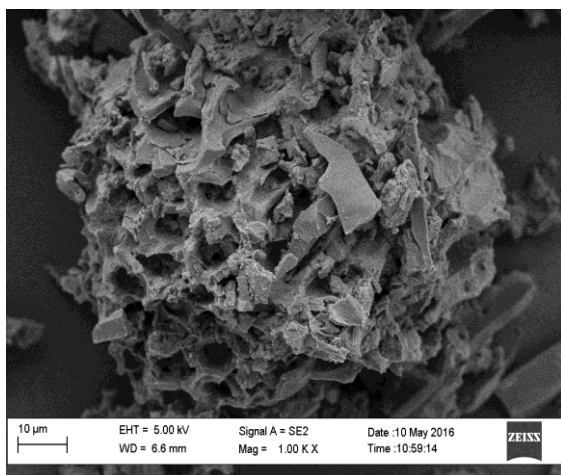


Figure 3ac: SEM micrograph of MAG-AC (1:3)

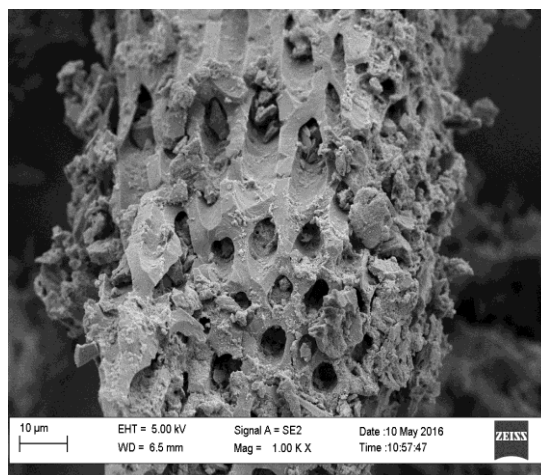


Figure 3d: SEM micrograph of MAG AC (1:5)

Transmission Electron Microscopy (TEM)

TEM is a microscopic technique which provides the fine detail of the particle size presents in the sample as small as a single column of atoms.

The TEM micrographs of magnetite at different magnification as shown in Figure 4a & b below reveal a rod-like shaped particle with ranges of diameter, the

particle is seen to have smooth surface which could enhance adsorption properties, which complement result obtained from SEM. This result is different from the one reported by Zhao et al.,2008⁴⁵ in which the magnetite nanoparticles have cubic shape which are uniform and mono-dispersed.

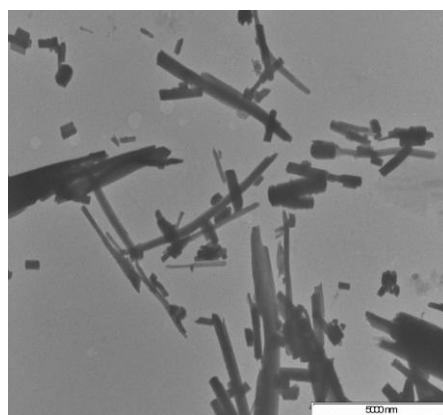
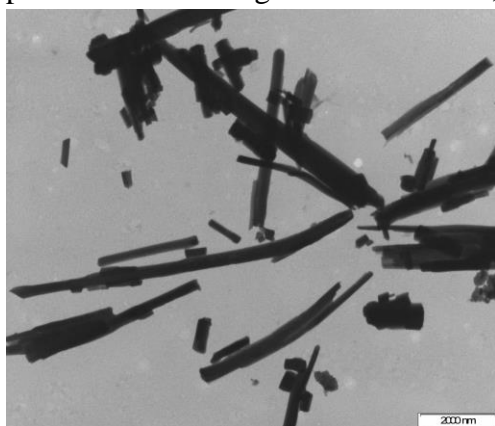


Figure 4: TEM micrograph of magnetite

Energy Dispersive X-ray Spectroscopy Analysis (EDS)

This instrumental technique was used to investigate the elemental composition of the adsorbents. Its characteristic ability is due to the fundamental principle that each has a unique atomic structure allowing unique set of peaks on its X-ray emission⁴⁶. From the Table 3 shown below, the major elements present in MAG and composites were observed to be C, O and Fe while the minor elements are Ca, Pd, Cl and Au. On

the other hand, C and O dominate the ACT sample. It can be observed that iron and oxygen are dominant in magnetite while Carbon is included in the composites. The peaks are more intense in the magnetite than the composites; this is due to crystal nature of magnetite.

The result of the particle size analyzer (Fig 6a-c) revealed that the sizes of different adsorbents are in the range 1-1000 nanometers.

Table 3: Elemental composition of adsorbents

Elemental Composition (%)											
Adsorbents	C	O	Fe	Ca	Pd	Cl	P	K	Ca	Au	Total
MAG	9.86	46.53	41.81	-	0.50	-	-	-	-	1.31	100
ACT	78.58	19.01	-	-	-	-	1.51	0.35	0.19	0.35	100
MAG-AC (1:3)	55.34	4.04	40.42	-	-	-	-	-	-	0.2	100
MAG-AC (1:5)	72.77	19.09	7.12	0.14	0.21	0.36	-	-	-	0.37	100

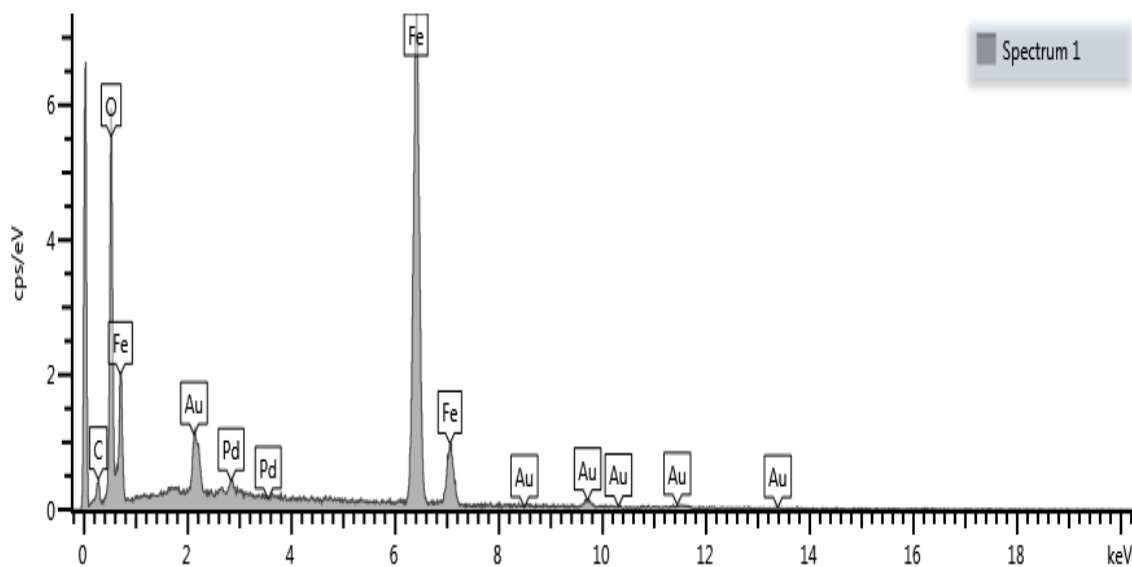


Figure 5a: EDX spectrum of magnetite

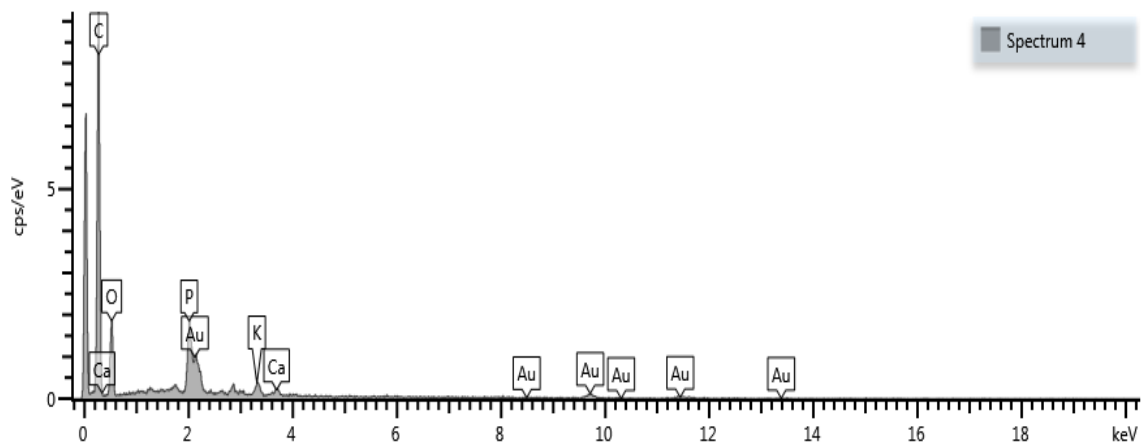


Figure 5b: EDX spectrum of Activated carbon

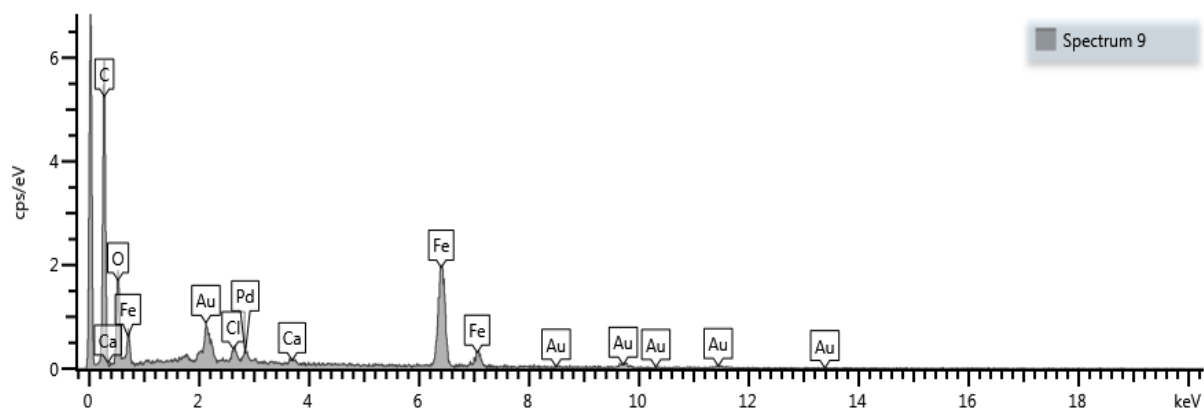


Figure 5c: EDX spectrum of MAG-AC (1:3)

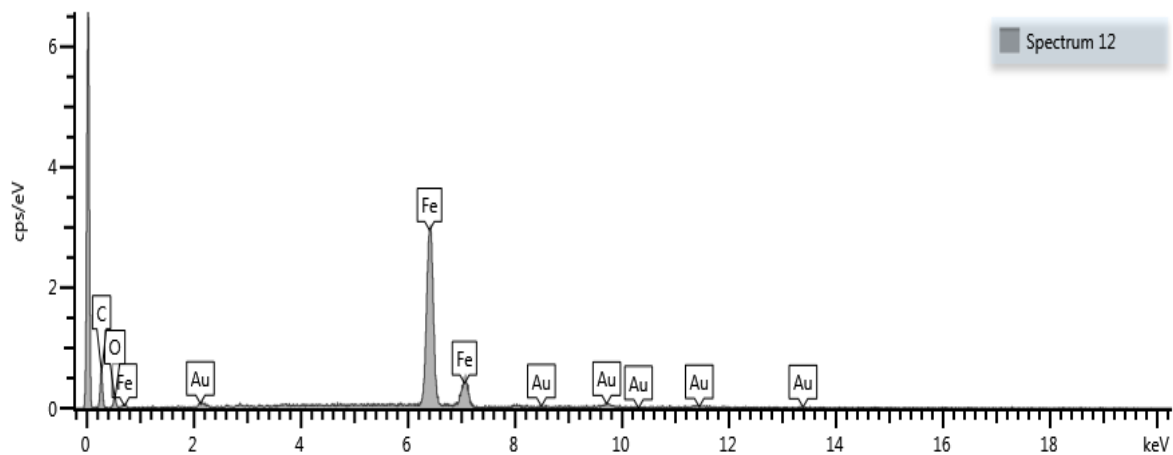


Figure 5d: EDX spectrum of MAG-AC (1:5)

Nanosizer Results

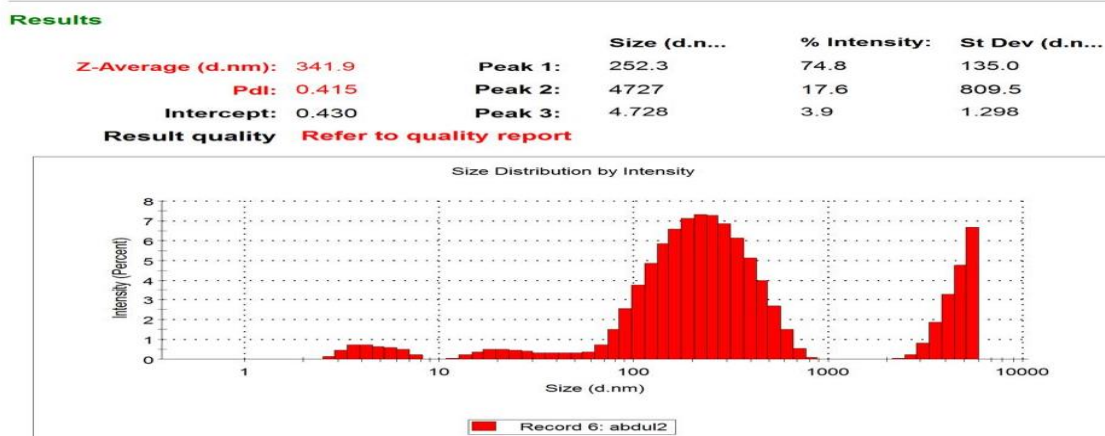


Figure 6a: Nanosizer chat of ACT by intensity

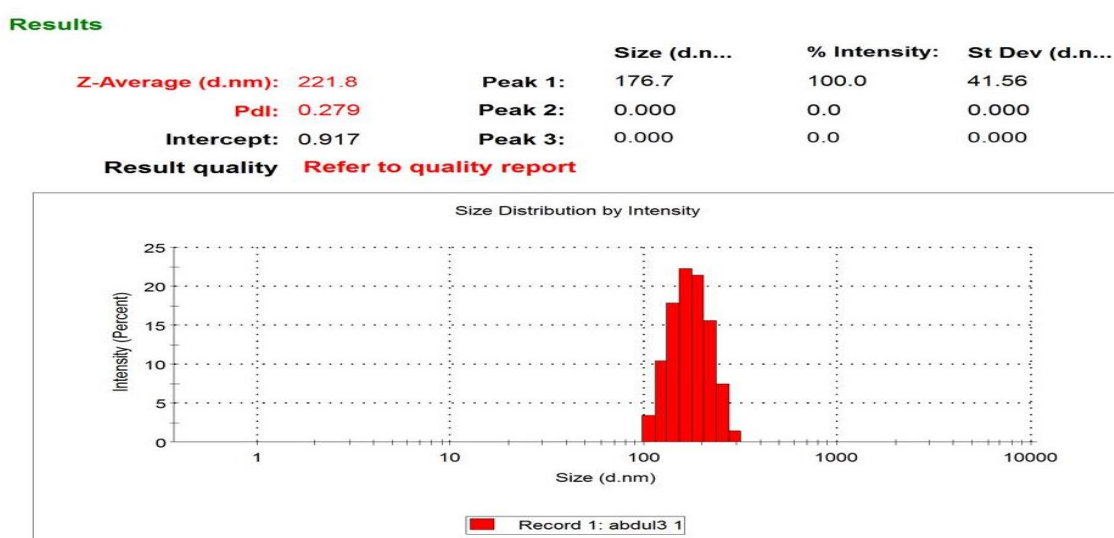


Figure 6b: Nanosizer chat of MAG-AC (1:5) by intensity

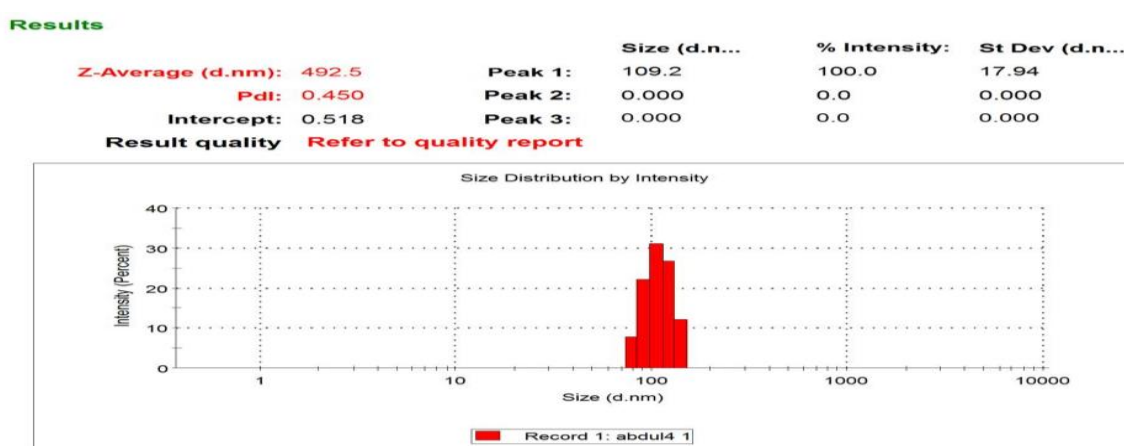


Figure 6c: Nanosizer chat of MAG-AC (1:3) by intensity

Results of the Adsorption Studies

The maximum absorption of sulphate anion was obtained at 362 nm. The calibration

curve of the standard solutions at 362 nm is shown in the Figure 6d.

Effect of Initial Concentration

The adsorption of sulphate ion from aqueous solution by all types of adsorbents synthesized at different initial concentration ranging from 5 - 800 ppm showed that the adsorption of sulphate ion (quantity adsorbed) increased with increase in initial concentration up to 500 ppm where the equilibrium was attained for all the adsorbents after which a drop occurred. This shows that the adsorption of sulphate ion is greatly dependent on the initial concentration. However, the increasing rate of sulphate ion adsorption decelerated with further increase in sulphate ion concentration. This behavior is due to the increase in the driving force of the concentration gradient, as further increase in the initial sulphate ion concentration

overcome the limitations of low adsorption by adsorbent⁴⁷.

It can be seen that the amount adsorbed in the $\text{SO}_4^{2-}/\text{MAG}$ system at equilibrium increased from 1.821 – 123.18 mg/g while adsorption capacity of $\text{SO}_4^{2-}/\text{ACT}$ and $\text{SO}_4^{2-}/\text{MAG-AC}$ (1:3) system also increased from 0.8454 – 65.58 mg/g and 1.8181 - 122.45 mg/g respectively. The maximum percentage adsorption onto the three adsorbents (MAG, ACT and MAG-AC (1:3)) was found to be 90.909 %, 84.54 and 90.909 % respectively. One can deduce from the results of percentage of sulphate ion adsorbed on the adsorbents that MAG and MAG-AC (1:3) performed better than ACT which could be as a result of sites been filled up as the concentration of sulphate ion increases in the aqueous solution⁴⁸.

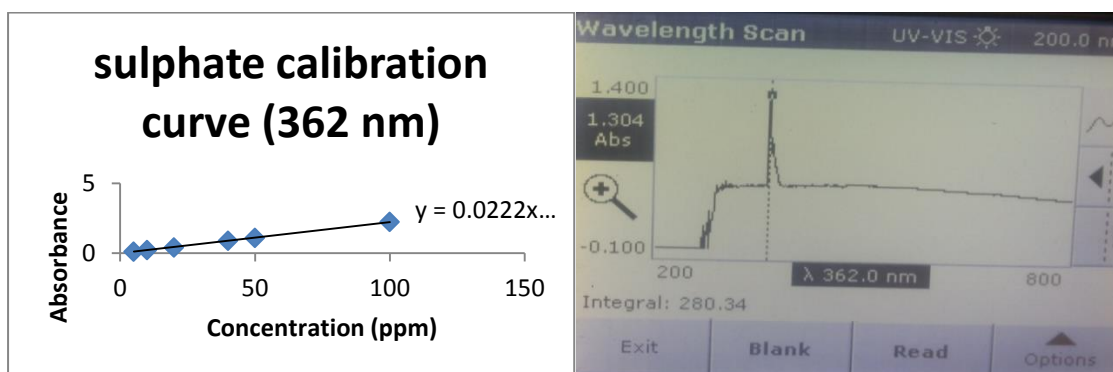


Figure 6d: Calibration curve for sulphate ion solution

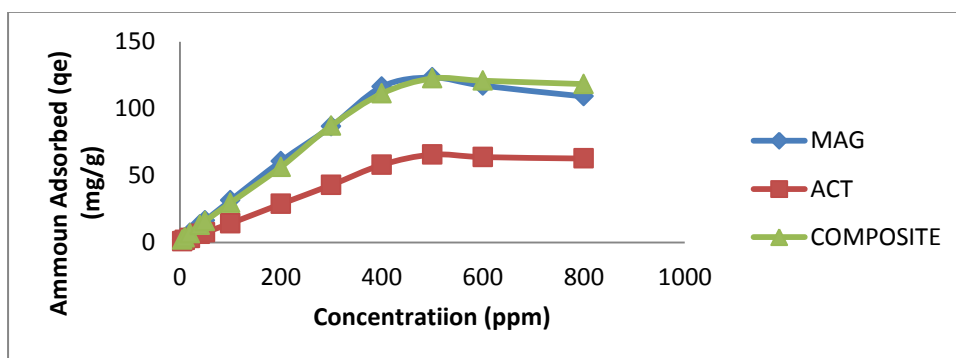


Figure 7a: Adsorption Profile diagram of sulphate ion adsorbed onto the adsorbents $V=25\text{cm}^3$, $T = 300\text{K}$ and time = 180mins

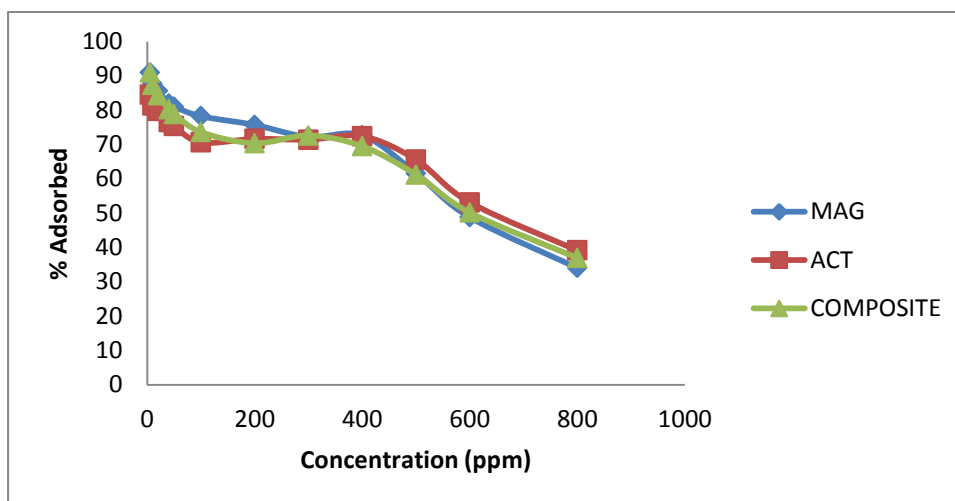


Figure 7b: percentage Profile diagram of sulphate ion adsorbed onto the adsorbents $V=25\text{cm}^3$, $T = 300\text{K}$ and time = 180mins

Effect of pH

The solution pH is one of the main effective parameters which could have a significant role in controlling the adsorption process [49]. The effect of pH on SO_4^{2-} adsorption is shown in Figure 8. As shown in this Figure, the maximum SO_4^{2-} removal on to MAG, ACT and MAG-AC (1:3) occurred at acidic pH of 5 at initial concentration of 500 ppm) with maximum percentage values of 91.34, 91.9 and 91.2 % respectively at pH 5. This can be due to the electrostatic attraction between the SO_4^{2-} anions and the positive charges located on the adsorbents surface. But, the fall in SO_4^{2-} removal as a result of

the rise in pH may be due to the fact that at higher pH, the adsorbents surface are negatively charged and subsequently enhances the electrostatic repulsion between sulphate ions and the adsorbents, leading to the release of the adsorbed species off the MAG, ACT and MAG-AC (1:3) surface⁵⁰. Since the maximum SO_4^{2-} adsorption was obtained at pH 5, this pH was selected as the optimum. This result is in good agreement with the previous studies in which the maximum adsorption uptake of sulphate ion occurred at acidic pH of 7 and 4^{51,27}.

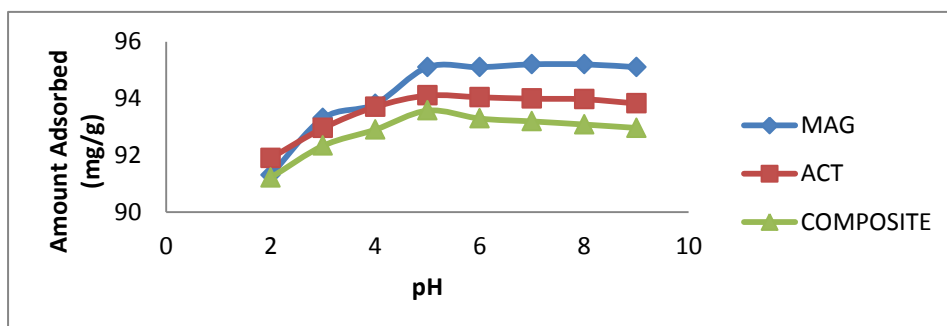


Figure 8: pH profile diagram for adsorption of sulphate on MAG, ACT and MAG-AC (1:3) ($V=25\text{cm}^3$, $T=300\text{K}$, Concentration= 500 ppm)

Effect of Adsorbent Dosage

The optimum amount of the adsorbent which can remove sulphate ions from aqueous solution was found through a batch-mode sorption. In due course, various amounts (0.02–0.5 g) of MAG, ACT and MAG-AC (1:3) were examined at 500 ppm optimized for the initial concentration and the sulphate ion removal efficiency as a function of adsorbents dosage was monitored. It was shown that as the adsorbent dosage increases, the sulphate removal percentage also increases while the quantity adsorbed decrease rapidly for all the adsorbents. This could be explained by the fact that an increase in the adsorbent dose may increase the accessibility of the active sites on the pores

of the adsorbents for the sulphate ions, which leads to an enhancement in the removal efficiency. This result is in agreement with the reports of some researchers^{27, 52}. Maximum adsorption capacity was therefore achieved using 0.01g mass of adsorbent. As shown in Figure 9a, by increasing adsorbents dosage from 0.01 to 1 g, the adsorption percentage of sulphate increased from 82.70 – 95.21 %, 83.38 - 95.37 %, and 80.80 – 93.75 % while the quantity adsorbed decrease from 418.54 – 19.04 mg/g, 416.90 – 19.07 mg/g and 404 -18.75 mg/g for MAG, ACT and MAG-AC (1:3) respectively at optimized condition.

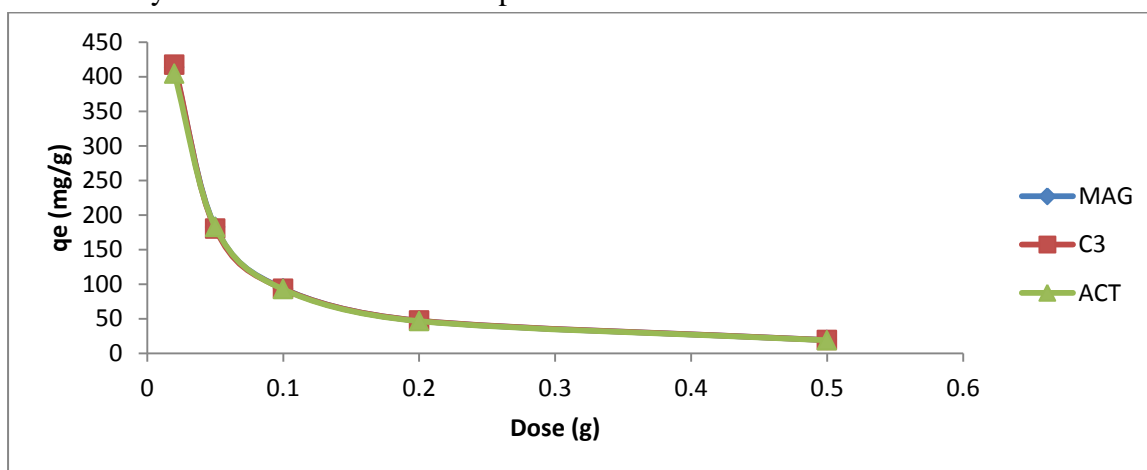


Figure 9a: Dose profile diagram for adsorption of sulphate on MAG, ACT and MAG-AC (1:3) system (V=25ml, T= 300k, Concentration =500 ppm, time= 180 mins, pH=5.0)

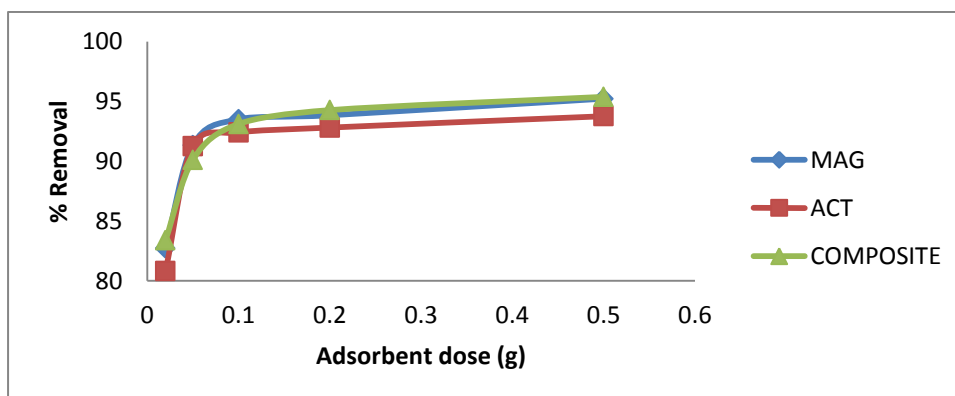


Figure 9b: % Dose removal profile diagram for adsorption of sulphate on MAG, ACT and MAG-AC (1:3) system (V=25ml, T= 300k, Concentration =500 ppm, time= 180 mins, pH=5.0)

Effect of Contact Time

Adsorption is a time dependent process and it is very important to know the rate of adsorption for designing and evaluating the adsorbent in removing contaminants from waste water.

The effect of contact time on the adsorption of sulphate ion onto MAG, ACT and MAG-AC (1:3) respectively are shown in Figure 10. The rates of sulphate ion adsorption on MAG, ACT and MAG-AC (1:3) from aqueous solution were described as quantity adsorbed as a function of contact time as shown in Figure 10. It can be observed that the adsorption capacity of the oxyanion increased with increasing time. The adsorption process can be classified into two portions representing fast and slow. The rapid increase may be as a result of vacant adsorption on sulphate sites. However, gradual reduction in the rate showed that adsorption sites have become saturated and

the ease of adsorption becomes more difficult until the adsorption reached equilibrium. Similar result was also reported in the literature⁵³. It can be observed that the amount adsorbed increases with increase in contact time to a point after which equilibrium was reached at 120 min for magnetite (MAG), 45 min for activated carbon (ACT) and 60 min for magnetite-activated carbon composite (MAG-AC (1:3)) with the maximum adsorption capacities in the range 91.1 – 96.44 mg/g respectively. The differences in the time of equilibrium may be due to the nature of the adsorbents. A time of 45 - 120 minutes adsorption time was selected as the equilibrium time for MAG, ACT and MAG-AC 1:3 respectively based on the results of the contact time studied and was used for further adsorption studies in investigating other parameters.

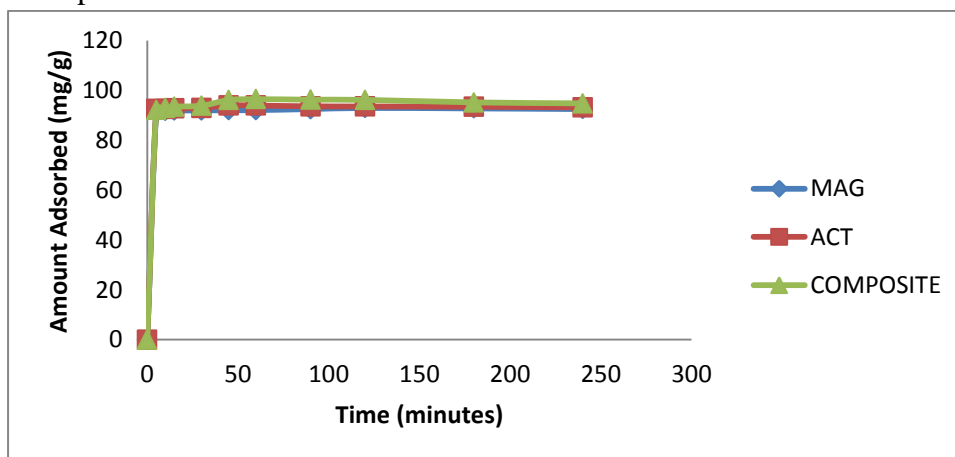


Figure 10: Time profile diagram for adsorption of sulphate on MAG, ACT and MAG-AC (1:3) ($V=25\text{cm}^3$, $T=300\text{K}$, Concentration=500 ppm, dose= 0.1g, pH=5.0)

Effect of Temperature

Normally temperature estimates the molecules, functional groups and surface morphology of the adsorbent and metals during adsorption processes. To determine the thermal effect of the various sorption

systems, adsorption studies were carried out at temperatures of 303 – 343 K. The temperature profile diagram for the adsorption system of sulphate ion onto MAG, ACT and MAG-AC (1:3) are shown

in Figure below. The plots show an increase in adsorption capacity with increase in temperature for all adsorbents. These results affirm the endothermic nature of the adsorption process. The endothermic nature may be attributed to an increase in the kinetic energy of the sulphate ions as

the anion moving faster to adsorbents surface or the anion are solvated [54]. Maximum adsorption capacity was achieved at 343K for MAG, ACT, and MAG-AC (1:3) at optimized condition. The adsorption capacity ranges from 7.39 and 38.77 mg/g

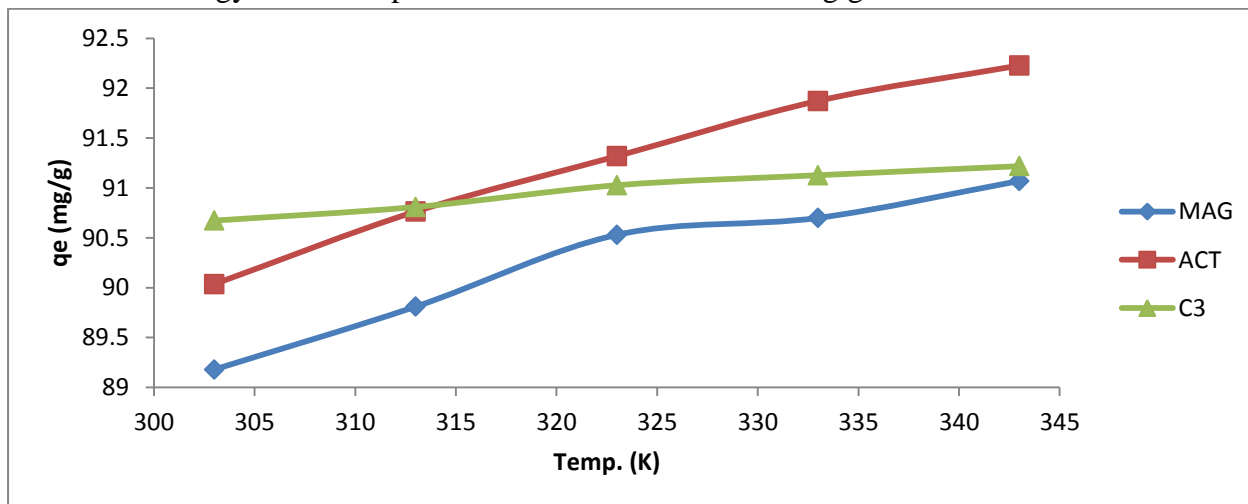


Figure 11: Temperature profile diagram of MAG, ACT and MAG-AC (1:3) ($V=25\text{cm}^3$, Concentration =500 ppm, dose=0.1g, pH=5.0, time = 120, 45 and 60 minutes respectively).

Adsorption Isotherms

In this study, Langmuir, Freundlich and Temkin isotherm models were used to describe the relationship between the amounts of sulphate ion adsorbed and its equilibrium concentration in solution has been studied and results are shown in Figure 12(a – c)

The Langmuir isotherm assumes that the uptake of sulphate ions occur on a homogenous surface by monolayer adsorption without any interaction between adsorbed ions. Once a site is filled, no further sorption can take place at that site

As such the surface will eventually reach a saturation point where the maximum adsorption of the surface will be achieved. The linear form of Langmuir isotherm model is given by the following equation:

$$\frac{C_e}{q_e} = \frac{1}{bq_m} + \left(\frac{1}{q_m}\right)C_e \quad (5)$$

Where q_e is the amount of adsorbate adsorbed at the time of equilibrium (mg/g), C_e is the equilibrium liquid-phase concentration of adsorbate in solution (mg/L), q_m is the maximum adsorption capacity (mg/g) and b is the Langmuir constant related to the energy of adsorption (L/mg). The Langmuir constants K_L and q_{\max} were calculated from the equation 5 and also an essential characteristic of Langmuir isotherm could be expressed from the dimensionless constant called equilibrium parameter

$$R_L = \frac{1}{1+K_L C_0}$$

Where K_L is the Langmuir constant and C_0 is the initial concentration (mg/L). The value of R_L indicates the adsorption nature to be

either unfavourable if $R_L > 1$), linear if $R_L = 1$, favourable if $0 < R_L < 1$ and irreversible if $R_L = 0$. The Langmuir separation factor

R_L , indicates the nature of the adsorption process as given in Table 4.

The obtained values regarding the Langmuir, isotherms for sulphate ion adsorption on to MAG, ACT and MAG-AC (1:3) are shown in Table 4 above. The correlation coefficient range from 0.954 - 0.979 were obtained for sulphate ion removal onto all the adsorbents.

This showed that the adsorption systems fitted Langmuir isotherm. The q_m of the

adsorbents were obtained to be in the range 83 - 142.86 mg/g while the Langmuir constant (b) were in the range 0.0028 - 0.016 L/mg, respectively. The value of R_L was observed to be in the range 0.199 - 0.676 which lies between 0 - 1, indicating that the adsorption process is favorable.

The linear plots of Langmuir equilibrium concentration C_e/q_e versus C_e are shown in the Figures 12a for sulphate ions sorption, for all the adsorbents used.

Table 4: Isotherms parameters for various sulphate ion adsorption processes

Adsorption Models	Isotherms Parameters	MAG	ACT	MAG-AC (1:3)
Langmuir	Q_{max} (mg/g)	125	83	142.86
	$b(K_L)$ (L/mg)	0.0028	0.0019	0.016
	R_L	0.586	0.676	0.199
	R^2	0.979	0.954	0.974
Freundlich	K_f	3.625	0.981	3.310
	$n, 1/n$	1.540, 0.649	1.201, 0.832	1.512, 0.661
	R^2	0.961	0.996	0.975
Temkin	K_T	0.669	0.406	0.585
	B	20.64	12.20	21.06
	R^2	0.860	0.849	0.854
	b_T	122.05	206.51	119.63

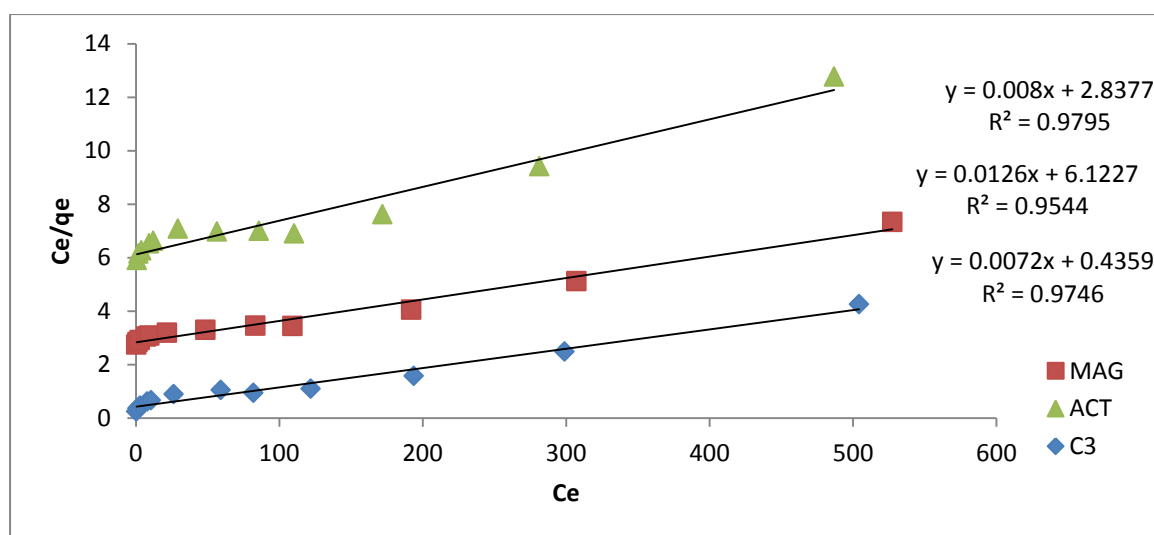


Figure 12a: Langmuir Isotherm of sulphate ion onto MAG, ACT and MAG-AC (1:3)

Freundlich Adsorption Isotherm

Freundlich isotherm is widely applied in heterogeneous systems especially for
Nigerian Journal of Chemical Research

organic compounds or highly interactive species on activated carbon and molecular sieves. The slope ranges between 0 and 1 is

a measure of adsorption intensity or surface heterogeneity, becoming more heterogeneous as its value gets closer to zero. Whereas, a value below unity implies chemisorption process where $1/n$ above one is an indicative of cooperative adsorption (physi-sorption)⁵⁶.

$$\ln q_e = \ln K_f + \frac{1}{n} \ln C_e \quad (6)$$

where the slope = $1/n$ and intercept = $\ln K_f$, q_e is the amount of solute adsorbed at equilibrium time in mg/g, C_e is the equilibrium concentration of adsorbate (mg/L), K_f is the capacity of adsorbent (mg/g) and n is the Adsorption constant (>1) for Freundlich (L/mg)

As it can be seen in the table above, the values of $1/n$ are between 0.649 - 0.832 while n values are in the range of 1.201 – 1.540. These value lies between $1 < n < 10$ indicating that the sorption of sulphate ion are favourable. The values of K_f were calculated to be in the range 1.072 - 1.919 for the three adsorbents. The R^2 values were found to be between 0.961- 0.996 which showed that sulphate ion fitted multilayer adsorption on heterogeneous surface for the three adsorbents and the extent is in the order of ACT > MAC-AC (1:3) > MAG.

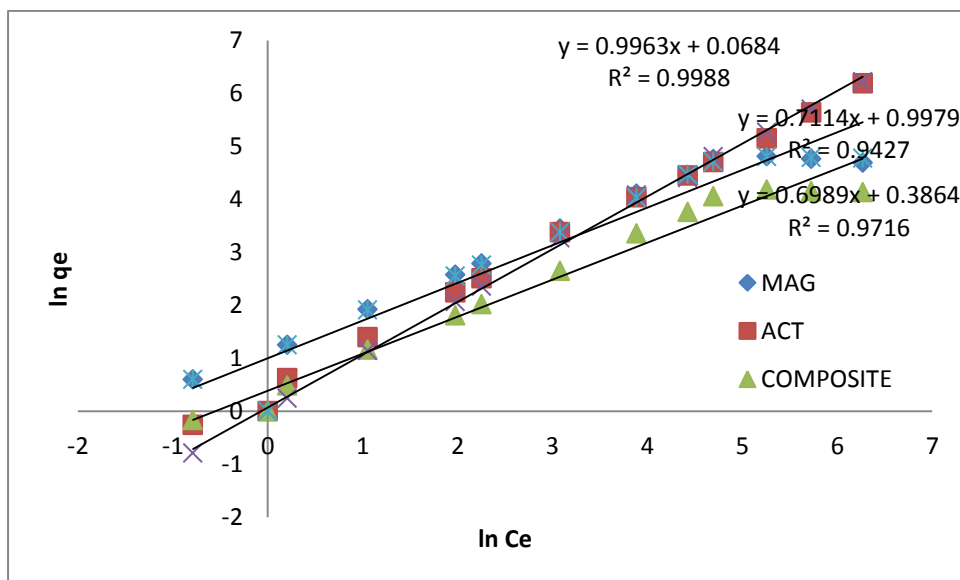


Figure 12b: Freundlich Isotherm of sulphate ion onto MAG, ACT and MAG-AC (1:3)

Temkin Adsorption Isotherm Model

The Temkin isotherm model assumes that the adsorption energy decreases linearly with the surface coverage due to adsorbent-adsorbate interactions. The Temkin isotherm model is given by the following equation⁵⁷.

$$Q_e = \frac{RT}{b_T} \ln(A_T C_e) \quad (7a)$$

$$Q_e = \frac{RT}{b_T} \ln A_T + \frac{RT}{b_T} \ln C_e \quad (7b)$$

Where $B = \frac{RT}{b_T}$

$$Q_e = B \ln A_T + B \ln C_e \quad (7c)$$

A_T = Temkin isotherm equilibrium binding constant (L/g)

b_T = Temkin isotherm constant

R = universal gas constant (8.314J/mol/K)

T = Temperature at 298K.

B = Constant related to heat of sorption (J/mol)

The values of K_T and B were calculated from the intercept ($B \ln K_T$) and slope (B) from the plot of $\ln C_e$ vs q_e . The K_T calculated values are in the range 0.406 – 0.669 and B values are in the 12.20 – 21.06 for ACT, MAG and MAG-AC (1:3) systems. These low values of the binding energies and heat of adsorption of the four systems indicate physical adsorption (Dada et al, 2012). The R^2 values (0.860, 0.854 and 0.849 for MAG, MAG-AC (1:3) and ACT respectively) showed that the three

systems fitted into the isotherm model with the MAG being the fittest and ACT being the least.

The adsorption of SO_4^{2-} /ACT fitted best into the Freundlich adsorption isotherm than the other two models used with the R^2 value of 0.996 while SO_4^{2-} /MAG fitted with Langmuir as seen in the data analysis above. The order of the isotherm fitness to the systems are in order of Freundlich > Langmuir > Temkin. It can be deduced from the three isotherms used that Freundlich fitted best for sulphate ion system.

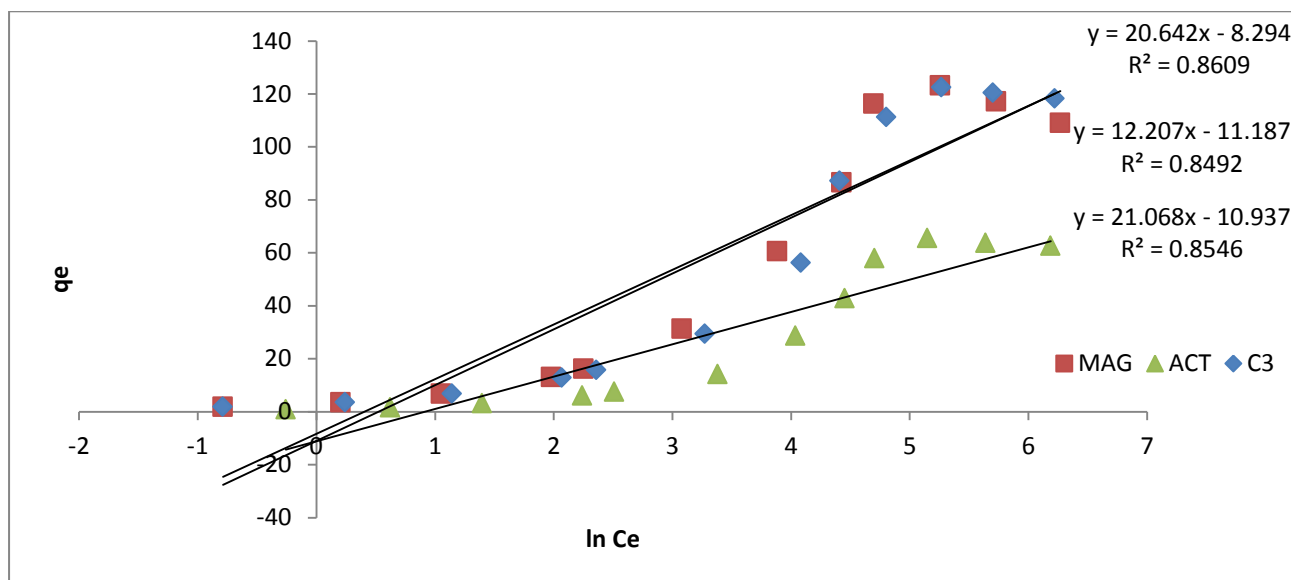


Figure 12c: Temkin Isotherm sulphate ion onto MAG, ACT and MAG-AC (1:3)

Adsorption Kinetics Study

Pseudo First Order Kinetics

The sorption kinetics may be described by a linear pseudo-first order equation:

$$\ln(q_e - q_t) = \ln q_e - K_1 t \quad (8)$$

Where q_t and q_e are the amounts of solute adsorbed at time t and equilibrium (mg/g), respectively, and K_1 is the pseudo-first order rate constant for the adsorption process (min^{-1}).

The slopes and intercepts of $\ln(q_e - q_t)$ versus t are used to determine the first order rate constant k_1 and the amount of metal or oxyanion adsorbed at equilibrium q_e .

The Lagergren's Pseudo first order plot of t (mins) versus $\ln(q_e - q_t)$ for sulphate ion system were all linear as it can be seen in the figure below with the correlation coefficient R^2 values that ranges between 0.818 - 0.947 for all adsorbents synthesized but the q_e (cal) were not in agreement with the q_e (exp)

values as q_e calculated values were very low compared to q_e experimental values. This suggests that this adsorption system is not a pseudo-first order reaction.

Pseudo-Second Order Kinetics

The linear pseudo-first order equation is

$$\frac{t}{q_t} = \frac{1}{K_2 q_e^2} + \frac{1}{q_e} t \quad (9)$$

Where q_e and q_t have the same meaning as above, K_2 is the rate constant of pseudo-second order adsorption ($\text{g mg}^{-1} \text{min}^{-1}$). The slopes and intercepts of t/q_t versus t are used to determine the second order rate constant K_2 and the amount of oxyanion adsorbed at equilibrium q_e .

The plot obtained for the pseudo-second order model represented better compared to the

pseudo-first order kinetic model as shown in Figure 13a. The pseudo second order kinetic plots are of better linearity with correlation coefficient of 1 (unity) for MAG and ACT while 0.999 which is almost close to unity for MAG-AC (1:3) system. The comparison between experimental and theoretically calculated q_e values for the sulphate ion adsorption onto the three forms of adsorbents as shown in Table 5 show a better agreement (very close) than in the pseudo first order model. This showed that pseudo-second order kinetic fitted better than the pseudo-first order kinetic for the adsorption of sulphate ion in aqueous solution by MAG, AC and MAG-AC (1:3) this is in agreement with literature on sulphate adsorption⁵¹. While Payman and Allan, 2009⁵² reported pseudo first order kinetic.

Table 5: Kinetics parameters for sulphate adsorption system

Kinetics Models	Parameters	MAG	ACT	MAG-AC (1:3)
Pseudo-first order	$Q_{e,cal}(\text{mg/g})$	1.479	1.54	6.80
	$Q_{e,exp}(\text{mg/g})$	92.90	93.93	96.45
	$K_1 (\text{min}^{-1})$	1.2×10^{-2}	1.4×10^{-2}	5.5×10^{-2}
	R^2	0.856	0.947	0.818
Pseudo-second order	$Q_{e,cal}(\text{mg/g})$	100	100	100
	$Q_{e,exp}(\text{mg/g})$	92.90	93.93	96.45
	$K_2 (\text{min}^{-1})$	1.0×10^{-1}	1.0×10^{-1}	5.0×10^{-2}
	R^2	1	1	0.999
Elovich	α		5.003	
	β	2.73	2.816	1.071
	R^2	0.831	0.613	0.593

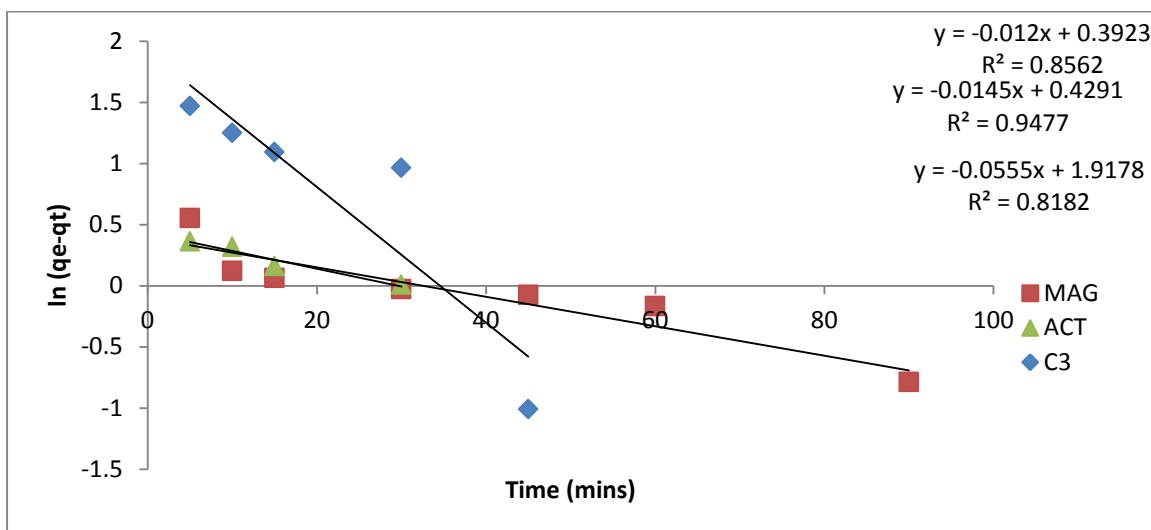


Figure 13a: Linearized plot of Pseudo-first order model plot of sulphate ion adsorption onto MAG, AC and MAG-AC (1:3)

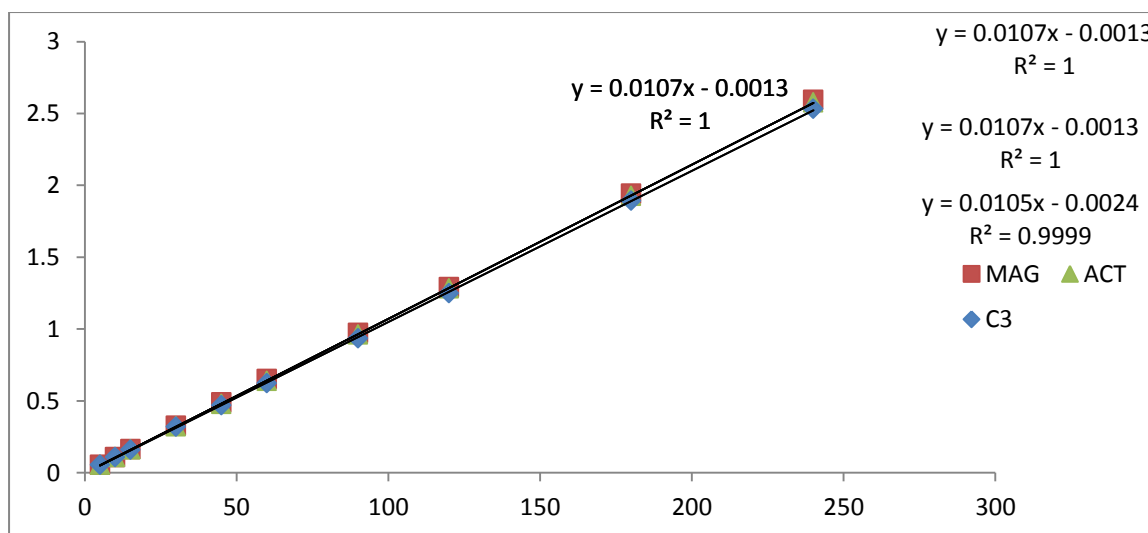


Figure 13b: Linearized plot of Pseudo-second order model plot of sulphate ion adsorption onto MAG, ACT and MAG-AC (1:3)

Elovich Kinetic Model

The Elovich equation is one of the most useful models for describing chemisorption on highly heterogeneous adsorbent [58]. The Elovich equation is generally expressed as:

$$\frac{dq}{dt} = \alpha e^{-\beta q} \quad (10a)$$

Where q is the sorption capacity at time t (mg/g), α is the initial adsorption rate (mg/g.min) and β is the desorption constant (mg/g.min) during any one experiment.

To simplify the Elovich equation assumed $\alpha \beta t \gg 1$ and by applying boundary

conditions $q_t = 0$ and $t = 0$ and q_t at $t = t$, equation 8a becomes:

$$\frac{1}{q_t} = \frac{\ln \alpha \beta}{\beta} + \frac{q \ln t}{\beta} \quad (10b)$$

Thus, if a plot of $1/q_t$ versus $\ln t$ is linearly correlated, the constants α and β are the slope and intercept respectively [59].

The correlation coefficient values obtained from the plots of the Elovich equation as shown in Table 5 above and Figure 13c below showed that the adsorption systems are in agreement with this kinetic model

since the $R^2 > 0.5$ for all the three adsorbents.

Pseudo second order kinetics fitted best among the three kinetics subjected to this

sorption system (sulphate ion system). This is also in agreement with the literature as it has been discussed.

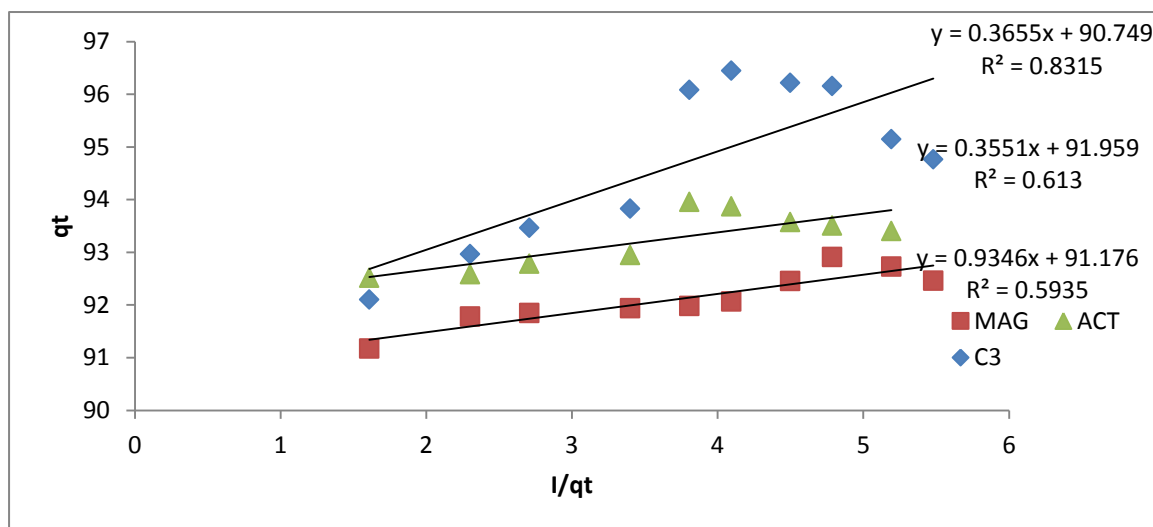


Figure 13c: Linearized plot of Elovich model plot of Sulphate adsorption onto MAG, ACT and MAG-AC (1:3).

Adsorption Thermodynamics

The thermodynamics for the adsorption of sulphate ion on to MAG, ACT and MAG-AC (1:3) was investigated in the range 303-343 K and the influence of temperature on the adsorption under the optimized conditions was studied. Thermodynamic parameters such as free energy (G), enthalpy (H) and entropy (S) changes during adsorption were evaluated from below equations.

$$K_c = \frac{q_e}{C_e} \quad (11a)$$

$$G = -RT \ln K_c \quad (11b)$$

$$\log K_c = \left(\frac{S}{2.303R} \right) - \left(\frac{H}{2.303RT} \right) \quad (11c)$$

Where K_c is the equilibrium constant, C_e is the adsorbate concentration at the equilibrium in mg/mol, ΔG , ΔH and ΔS are changes in Gibbs free energy, enthalpy and entropy in kJ/mol respectively. R is the gas constant and T is the temperature in Kelvin. The values of H and S was determined from the slope and the intercept of Van't Hoff plots of $\log K_c$ versus $1/T$.

Table 6: Thermodynamic parameter of adsorption of Sulphate ion onto MAG, ACT and MAG-AC (1:3)

Adsorption system	Temp (K)	ΔG (kJ/mol)	ΔH (kJ/mol)	ΔS (J/mol/K)	R^2
$\text{SO}_4^{2-}/\text{MAG}$	303	-5.314	4.573	32.73	0.969
	313	-5.663			
	323	-6.062			
	333	-6.305			
	343	-6.622			
$\text{SO}_4^{2-}/\text{ACT}$	303	-5.545	5.929	37.912	0.997
	313	-5.94			
	323	-6.319			
	333	-6.714			
	343	-7.054			
$\text{SO}_4^{2-}/\text{MAG-AC}$	303	-5.729	1.484	23.81	0.982
	313	-5.961			
	323	-6.222			
	333	-6.448			
	343	-6.674			

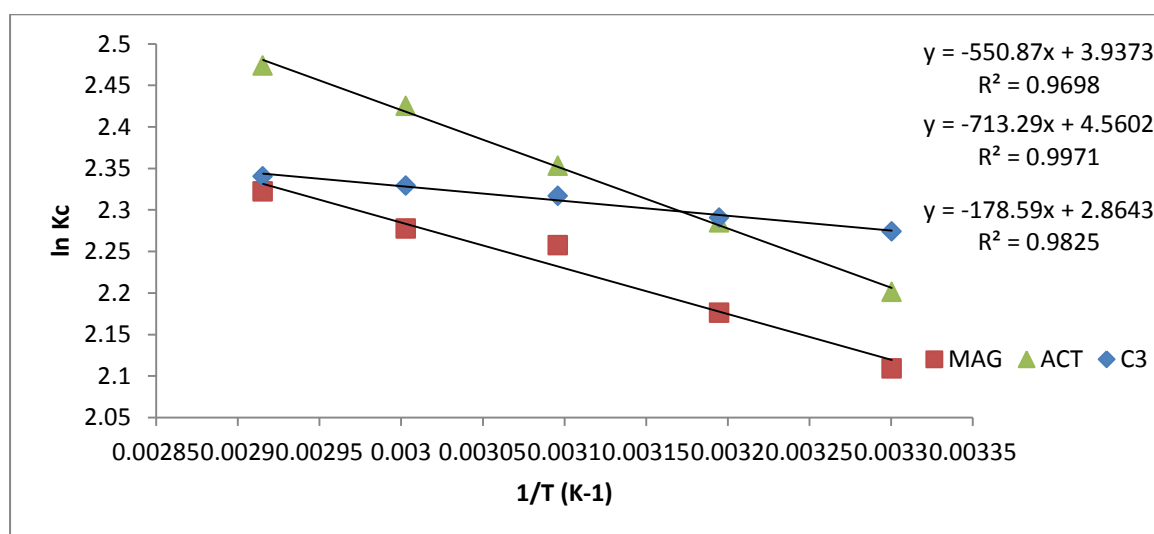


Figure 14: Thermodynamic plot of sulphate ion on to MAG, ACT and MAG-AC (1:3)

The Gibb's free energy (ΔG), enthalpy change (ΔH) entropy change (ΔS) and correlation coefficient R^2 obtained for the thermodynamic studies are shown in the table 6 above. It can be observed that (ΔG) values are negative in all systems. The

Gibb's free energy (ΔG), signify the degree of spontaneity of adsorption process. The negative value implies a feasible and a spontaneous reaction system over the temperature range studied.

It could be observed from the table above that ΔH values are all positive in the systems which confirmed the favourability of the processes. The lower values of ΔH suggest that the adsorption process is likely to be physisorption⁶⁰. However, the heats of adsorption in these systems were all endothermic.

The values of ΔS from the table above are positive. The ΔS is a measure of disorderliness of adsorption at adsorbent-adsorbate interface and the driving force.

The positive value of ΔS is an indication of an increased disorderliness and randomness at the solid-liquid interface of the system. Similar trend was reported in the literature⁵².

The corresponding correlation coefficient R^2 values for all the system are closer to unity which can also be found in the Table 6.

The comparison of the adsorption of sulphate with the adsorbents prepared in this study with some literature values using different adsorbents is shown in Table 7.

Table 7: Comparison of adsorption on sulphate using different adsorbents

Adsorbent	pH	Langmuir (R^2)	Freundlich	Q_m (mg/g)	Kinetics	Adsorbate	References
Magnetite	4	ND	ND	ND	Pseudo 2 nd order	Sulphate	Payman and Alllan, 2009
ACT	7	ND	ND	ND	Pseudo 2 nd order	Sulphate	Mohammed <i>et al.</i> , 2009
Ni-O MNP	7	0.9999	0.9916	ND	ND	Sulphate	Uzaira <i>et al.</i> , 2012
MAG	5	0.979	0.961	125	Pseudo 2 nd order	Sulphate	This study
ACT	5	0.954	0.996	83	Pseudo 2 nd order	Sulphate	This study
MAG-AC(1:3)	5	0.974	0.975	142.86	Pseudo 2 nd order	Sulphate	This study

CONCLUSION

Adsorption batch tests for sulphate (SO_4^{2-}) removal from aqueous solution by synthetic Fe_3O_4 nanoparticles, activated carbon and their composite (Fe_3O_4 -AC nano-composites) were studied. The adsorption studies results revealed R^2 value ranging from 0.961 - 0.996 for Freundlich and Langmuir isotherm ranges from 0.954 – 0.979 for all types of adsorbents studied. Pseudo-first-order kinetic models correlation coefficient factor ranges between 0.818 – 0.947 while Pseudo-second-order kinetic models R^2 values ranges from 0.999 - 1. The equilibrium time for all adsorbent types range from 45 - 120 minutes and the maximum monolayer capacity (q_{max}) were observed to be

between 83.0 - 142.86 mg/g for all the adsorbents at optimum pH 5. Thermodynamic studies revealed that the adsorption system was feasible, spontaneous and endothermic.

ACKNOWLEDGMENTS

The authors wish to thank the Department of Chemistry, University of Ilorin, Nigeria for providing an enabling environment to carry out this research work. Also the Nanotechnology Laboratory, Federal University of Technology, (FUT), Minna, Niger State –Nigeria for assisting in carrying out BET surface area analyses and Department of Chemistry, University of York, United Kingdom for

assisting in the SEM and TEM analyses of the prepared samples.

REFERENCES

1. Dave P.N., Pauline L. S. and David G. K. *Source and behaviour of arsenic in natural waters*. British Geological Survey, Wallingford, Oxon OX10 8BB, U.K. 261(2002)
2. Sugimoto T., Wang Y. J. *Mechanism of the shape and structure control of monodispersed α -Fe₂O₃ particles by sulphates ions*. Colloid Interface Sci. 207, 137–149 (1998)
3. Greenwood N.N., Earnshaw A. *Chemistry of elements*. 2nd edition, Oxford, pergamon press. (1984)
4. Kadirvelu K., Namasivayam C., *Activated carbon from coconut coirpith as metal adsorbent: adsorption of Cd (II) from aqueous solutions*. Adv. Environ. Res. 7, 471–478 (2003)
5. Omar, W., Al-Itawi H., *Removal of Pb²⁺ ions from aqueous solutions by adsorption on kaolinite clay*. Am. J. Appl. Sci. 4(7), 502–507 (2007)
6. Amer M.W., Khalili F.I., Awwad A.M. *Adsorption of lead, zinc and cadmium ions on polyphosphate-modified kaolinite clay*. J. Environ. Chem. Ecotoxicol. 2(1), 001–008 (2010)
7. Su W., Zhou L., Zhou Y. *Preparation of microporous activated carbon from raw coconut shell by two steps procedure*. Chin. J. Chem. Eng. 14(2), 266–269 (2006)
8. Pehlivan E., Altun T., Paravici S., *Utilization of barley straws as biosorbents for Cu²⁺ and Pb²⁺ ions*. J. Hazard. Mater. 164, 982–986 (2009)
9. Abdus-Salam N., Adekola F.A. *Comparative dissolution of natural goethite samples in HCl and HNO₃*. JASEM 10(2), 11–17 (2006)
10. Abdullah M. Al-Enizi, Ahmed A. Elzatahry, Mariam A. AlMaadeed, Jinxiu Wang, Dongyuan Zhao, Salem Al-Deyab. *Synthesis and electrochemical properties of nickel oxide/carbon nano-fiber composites*. Carbon, 71, 276-283. (2014)
11. Amin R.S., Elzatahry A.A., El-Khatib K.M., Youssef M.E. *Nanocatalysts prepared by microwave and impregnation methods for fuel cell*. Int. J. Electrochem. Sci, 6, 4572-4580. (2011)
12. Salah El-Din T.A., Elzatahry A.A., Aldhayan D.M., Al-Enizi A.M. and Al-Deyab. S.S. *Synthesis and characterization of magnetite zeolite nanocomposite*. Int. J. Electrochem. Sci., 6, 6177 – 6183 (2011)
13. Wang Y., Tang J., Peng Z., Wang Y., Jia D., Kong B. *Fully solar-powered photo electrochemical conversion for simultaneous energy storage and chemical sensing*. NanoLett. 14, 3668–3673 (2014)
14. Zhang T., Surampalli R., Lai K., Hu Z. *Nanotechnologies for water environment applications*. Amer Society of Civil Engineers. (2009).
15. Babak K., Roshanak R., Kalantary., Ahmad J., Jafari S., Ahmad A., Ali E. and Ali A. *Pb(II) Adsorption onto a Magnetic Composite of Activated Carbon and Superparamagnetic Fe₃O₄ Nanoparticles*. *Experimental and Modelling Study*, 43(8), 1157–1166. (2015)
16. Montane D, Torne-Fernandez VF. *Activated carbons from lignin: kinetic modeling of the pyrolysis of Kraft lignin activated with phosphoric acid*. Chemical Engineering Journal, 106(1), 1-12 (2005)

17. Jean-Pierre J, Corinne C and Elisabeth T. *Iron oxide chemistry. From molecular clusters to extended solid networks*. Chemical Community, 5, 481-483. (2004)
18. Do, M., Phan, N. and Nguyen T. *Activated carbon/Fe₃O₄ nanoparticle composite: Fabrication, methyl orange removal and regeneration by hydrogen peroxide*. Chemosphere. 85, 1269–1279. (2011) doi: 10.1016/j.07.023
19. APHA, *Standard Methods for the Examination of Water and Wastewater*, 20th Edition. Method 4500E
20. Sawyer, C. N., McCarty, P. L., and Parkin, G. F. *Chemistry for Environmental Engineering*. Fourth Edition, McGraw-Hill, Inc., New York (2000)
21. Roshanak R. K., Emad D., Anoushiravan M., Leila R., Ali E., Babak K. and Ali A. *Nitrate adsorption by synthetic activated carbon magnetic nanoparticles: kinetics, isotherms and thermodynamic studies. Desalination of water treatment*. Taylor and Francis (2015)
DOI:10.1080/19443994.2015.1079251
22. Azizian S. *Kinetics models of sorption: a theoretical analysis*. Journal of colloid and interface science, 276, 47-52 (2004)
23. Lori, J. A. Lawal, A.O. and Ekanem, E.J. *Proximate and ultimate analyses of bagasse, sorghum, and millet straws as precursors for active carbons*. Journal of Applied Science Volume 7 (21), 3249-3255 (2007).
24. Malik R., Ramate D.S., Wate S.R. *Adsorption of malachite green on groundnut shell waste based powdered activated carbon*. Waste Management, Volume 27, Issue 9, Pages 1129-1138 (2006)
25. Olowoyo, D. N. and Orere, E. E. *Preparation and characterization of activated carbon made from palm-kernel shell, coconut shell, groundnut shell and obeche wood (Investigation of apparent density, total ash content, moisture content, particle size distribution parameters)*. International Journal of Research in Chemistry and Environment, Vol. 2, No. 3, 32-35 (2012)
26. Bansode, R. R., Losso, J. N., Marshall, W. E., Rao, R. M., & Portier, R. J. *Adsorption of metal ions by pecan shell-based granular activated carbons*. Bioresource Technology, 89, 115–119 (2003)
27. Mohammed M. A., Babagana G. and Bitrus K. H. *Production and Characterization of activated carbon from groundnut shell sourced in Maiduguri*. Columban Journal of Life Science 17 (1) 18-24 (2015)
28. Jibril B., Maamari R., Houache O., Aamri M. and Qalhati, M. *Effect of H₃PO₄ and KOH on Pyrolysis of Bituminous Coal in Preparation of Activated Carbon*. Journal of applied sciences Research, 3 (11), 1343 – 135 (2007)
29. Raffiea, B. J., Palanisamy, P. N and Sivakumar, P. *Preparation and Characterization of Activated carbon from thevetia peruviana for the removal of dyes from textile waste water*. Advances in Applied Science Research, 3(1), 377-383 (2012)
30. Aziz A., Ouali M.S., Elandaloussi el H., De Menorval L.C., Lindheimer M. *Chemically modified olive stone: a low-cost sorbent for heavy metals and basic dyes removal from aqueous solutions*. Journal of Hazard Material, 163, 441-447. (2009)
31. Baccar R., Bouzid J., Feki M., Montiel A. *Preparation of activated carbon from Tunisian olive-waste cakes and its application for adsorption of heavy metal ions*. Journal of Hazard Material, 162, 1522-1529. (2009)
32. Subbaiah M.V., Yuvaraja G., Vijaya, Y., Krishnaiah A. *Equilibrium, kinetic and thermodynamic studies on*

- biosorption of Pb(II) and Cd(II) from aqueous solution by fungus (Trametes versicolor) biomass.* Journal of Taiwan Institute of Chemical Engineering, 42, 965–971 (2011)
33. Mamindy-Pajany Y., Hurel C., Marmier N., and Romeo M. *Arsenic (V) adsorption from aqueous solution onto goethite, hematite, magnetite and zero-valent iron: Effects of pH, concentration and reversibility.* Desalination, 281, 93-99 (2011)
 34. Ghazy S.E., El-Morsy S.M. *Sorption of lead from aqueous solution by modified activated carbon prepared from olive stones.* African Journal of Biotechnology, 8, 4140-4148. (2009).
 35. Martinez N.S., Fernandez J.F., Segura X.F., Ferrer A.S. *Pre - oxidation of an Extremely Polluted Industrial Wastewater by the Fenton's Reagent.* Journal of Hazardous Material, B101,315-322 (2003)
 36. Kosmulski M., maczka E., Jartych E., Rosenholm J.B. *Synthesis and characterization of goethite and goethite-hematite composite. Experimental study and literature survey.* Advance Colloid and interface Science, 103, 57-76 (2003)
 37. Gingasu D., Mindru I., Patron L.A., Calderon-Moreno J.M., Diamandescu L., Tuna F., Popescu T. *Investigation of magnetite formation in the presence of hydrazine dihydrochloride.* Digest Journal of Nanomaterials and Biostructures, 6, (3), 1065-1072 (2011)
 38. Chomchoey N. Bhongsuwan D., Bhongsuwan T. *Arsenic Removal from Synthetic Wastewater by Activated Carbon - Magnetic Nanoparticles Composite.* The 11th international conference on mining, materials and petroleum engineering, Paper ID 93 (2013)
 39. Babak K., Roshanak R., Kalantary., Ahmad J., Jafari S., Ahmad A., Ali E. and Ali A. *Pb(II) Adsorption onto a Magnetic Composite of Activated Carbon and Superparamagnetic Fe₃O₄ Nanoparticles.* Experimental and Modelling Study, 43(8), 1157–1166 (2015)
 40. Han Z., Sani B., Mrozik W., Obst W., Beckingham B., H.K. Karapanagioti H.K., Werner D. (2015). *Magnetite impregnation effects on the sorbent properties of activated carbons and biochars,* Water Resources. 70, 394–403.
 41. Zheng, Y., Zhu, Y., and Wang, A. *Kapok fiber structure-oriented polyallylthiourea: Efficient adsorptive reduction for Au(III) for catalytic application.* Polymer 55, 5211–5217. doi:10.1016/j.polymer.2014.08.040 (2014)
 42. Liu Z., Zhang F-S., Sasai R. *Arsenate removal from water using Fe₃O₄-loaded activated carbon prepared from waste biomass.* Chemical Engineering Journal, 160 57–62 (2010)
 43. Jung M., Ahn K., Lee Y., Kim K., Rhee J., Park J.T., Paeng K. *Adsorption characteristics of phenol and chlorophenols on granular activated carbon (GAC).* Microchemical Journal, 70 123–131 (2001)
 44. Tan I.A.W., Ahmad A.L., and Hameed B.H. *Preparation of activated carbon from coconut husk: Optimization study on removal of 2,4,6-trichlorophenol using response surface methodology.* Materials, 153, 709–717 (2008)
 45. Zhao Y, Qiu Z. and Huang J. *Preparation and Analysis of Fe₃O₄ Magnetic Nanoparticles Used as Targeted-drug Carriers,* Chinese Journal of Chemical Engineering, 16(3) 451—455 (2008)
 46. Joseph G. *Scanning Electron Microscopy and X-ray micro analysis.* Spring.ISBN 978-0-30647292-3 (2003)

47. Hamdi, H., De La Torre-Roche, R., Hawthorne, J., and White, J. C. *Impact of non-functionalized and amino-functionalized multiwall carbon nanotubes on pesticide uptake by lettuce (Lactuca sativa L.)*. *Nanotoxicology* 9, 172–180 (2015): doi: 10.3109/17435390.2014.907456
48. Bektas N. and Kara S. *Removal of lead from aqueous solutions by natural clinoptilolite: Equilibrium and kinetics studies*. *Sep. Purif. Technol.*, 39, 189–200 (2004)
49. Cho H-H, Wepasnick K, Smith BA, Bangash FK, Fairbrother DH, Ball W., (2009)., *Sorption of aqueous Zn [II] and Cd [II] by multiwall carbon nanotubes: the relative roles of oxygen-containing functional groups and graphenic carbon*. *Langmuir*, 26, 967–981.
50. Yuan P., Liu D., Fan M., Yang D., Zhu R., Ge F., Zhu J., He H. *Removal of hexavalent chromium [Cr (VI)] from aqueous solutions by the diatomite-supported/unsupported magnetite nanoparticles*. *Journal of Hazard Material*, 173, 614–621 (2010)
51. Uzaira R.1., Anum I., Abida K. K.. *Synthesis, Characterization and Application of Nanomaterials for the Removal of Emerging Pollutants from Industrial Waste Water, Kinetics and Equilibrium Model*. *Journal of Water Sustainability*, 2 (4) 233–244 (2012)
52. Payman R. and Allan H. *An ATR-FTIR study of sulphate sorption on magnetite; rate of adsorption, surface speciation, and effect of calcium ions*. *Journal of Colloid and Interface Science*, 333, 27–32 (2009)
53. Kakavandi B, Esrafil A, Mohseni-Bandpi A, Jafari AJ, Kalantary RR. *Magnetic Fe₃O₄-AC nanoparticles as adsorbents for removal of amoxicillin from aqueous solution*. *Journal of water Science and Technology*, 69, 147–155 (2014)
54. Naseem, R.; Tahir, S. S. *Removal of Pb (II) from aqueous/ acidic solutions by using bentonite as an adsorbent*. *Wat. Res.*, 35(16), 3982–3986 (2001)
55. Oliveira C.S., Vasconcellos M.C. Pinheiro J. *The population density effects on the reproductive biology of the snail Bradybaena similaris (Mollusca, Gastropoda)* *Braz. J. Biol.*, 68, 631–637 (2008)
56. Gimbert, F., Nadia M. C., François R., Pierre-Marie B. and Grégorio C. *Adsorption isotherm models for dye removal by cationized starch-based material in a single component system: error analysis*. *Journal of Hazard Material*, 157(1), 34-46 (2008)
57. Tempkin, M.I. Pyzhev, V. *Kinetics of ammonia synthesis on promoted iron catalyst*. *Acta Phys. Chim. USSR* 12, 327–356 (1940)
58. Aharoni C. and Tompkin F.C. *Rates of adsorption of hydrogen, carbon monoxide and their mixtures on zinc oxide*. *Trans. Faraday. SOC.* 66, 434 (1970).
59. Chien, S. H. & Clayton, W. R. *Application of Elovich equation to the kinetics of phosphate release and sorption in soils*. *Soil Sci. Soc. Am. J.* 44: 265–268 (1980)
60. Hema, M. and Arivoli, S. *Adsorption Kinetic and thermodynamics of malachite green dye into acid activated low cost carbon*. *J. App. Sci. Environ. Management.* 12(1), 43-51 (2000).